S-acylation of NLRP3 provides a nigericin sensitive gating mechanism that controls access to the Golgi

Daniel M. Williams[1]*, Andrew A. Peden[1]*

[1]School of Bioscience, University of Sheffield, Western Bank, Sheffield S10 2TN, UK

* Co-corresponding authors

daniel.williams@sheffield.ac.uk; a.peden@sheffield.ac.uk

Abstract

NLRP3 is an inflammasome seeding pattern recognition receptor activated in response to multiple danger signals which perturb intracellular homeostasis. Electrostatic interactions between the NLRP3 polybasic (PB) region and negatively charged lipids on the trans-Golgi network (TGN) have been proposed to recruit NLRP3 to the TGN. In this study, we demonstrate that membrane association of NLRP3 is critically dependant on S-acylation of a highly conserved cysteine residue (Cys-130), which traps NLRP3 in a dynamic S-acylation cycle at the Golgi, and a series of hydrophobic residues preceding Cys-130 which act in conjunction with the PB region to facilitate Cys-130 dependent Golgi enrichment. Due to segregation from Golgi localised thioesterase enzymes caused by a nigericin induced breakdown in Golgi trafficking, NLRP3 becomes immobilised on the Golgi through reduced de-acylation of its Cys-130 lipid anchor, suggesting that disruptions in Golgi homeostasis are conveyed to NLRP3 through its acylation state. Thus, our work defines a nigericin sensitive S-acylation cycle that gates access of NLRP3 to the Golgi.

Introduction

Inflammasomes are multimolecular complexes that control the initiation of inflammatory responses to various damage associated molecular patterns (DAMPs) and pathogen associated molecular patterns (PAMPs) (Chou et al., 2023). The core complex involved in the formation of an active inflammasome consists of a pattern recognition receptor (PRR), which sense various perturbations in intracellular homeostasis and are the trigger point for inflammasome activation, the adaptor protein ASC, which acts to amplify recognition of DAMPs and PAMPs by PRRs and ensure a robust and rapid response, and a final effector protein – Caspase-1, which, amongst other substrates, cleaves the pro-inflammatory cytokine interleukin-1-beta (IL-1β) and the pore forming protein Gasdermin-D into their bioactive forms. Due to its involvement in the pathogenesis of several diseases, including atherosclerosis (Duewell et al., 2010) and Alzheimer's disease (Heneka et al., 2013), one of the most well studied inflammasome seeding PRRs is NLRP3 (**N**ACHT, **L**R**R** and **P**YD domain containing protein **3**) (Akbal et al., 2022; Fu and Wu, 2023; Liang et al., 2021; Seoane et al., 2020; Swanson et al., 2019). Stimuli that trigger canonical NLRP3 activation are diverse, ranging from bacterial ionophores such as nigericin (Perregaux et al., 1992) to agents which damage lysosomal integrity (Duewell et al., 2010; Hornung et al., 2008). The majority of these stimuli are unified by their ability to deplete intracellular potassium, which has been proposed to be a common danger signal sensed by NLRP3 (Munoz-Planillo et al., 2013). Recent studies have revealed that NLRP3 is a peripheral membrane protein, recruited to the Golgi apparatus and endosomes through interactions between a highly conserved polybasic (PB) region within NLRP3 itself, and negatively charged phospholipids such as phosphatidylinositol-4-phosphate (PI4P) found in the cytoplasmic leaflet of intracellular membranes (Chen and Chen, 2018; Lee et al., 2023; Schmacke et al., 2022; Zhang et al., 2023). Membrane binding is important for formation of an inactive NLRP3 oligomer and an optimal response to NLRP3 stimuli (Andreeva et al., 2021; Chen and Chen, 2018), although how membrane binding and sensing of NLRP3 stimuli are linked is at present unclear.

The presence of a PB motif alone is often insufficient to allow stable membrane association. As one example directly relevant to NLRP3, basic residues within the hyper-variable region (HVR) at the C terminus of K-Ras4B, a membrane bound GTPase that mediates key signalling events from the plasma membrane (Zhou et al., 2018), are paired with a proximal lipid anchor to confer specific localisation to the plasma membrane, with neither module alone sufficient for plasma membrane binding (Choy et al., 1999; Hancock et al., 1991; Hancock et al., 1990). A working model for the steady state localisation of K-Ras4B at the plasma membrane posits that the farnesyl group provides an initial non-specific weak affinity for all intracellular cellular membranes. The PB region acts in concert with the farnesyl lipid anchor to allow K-Ras4B to preferentially partition to the plasma membrane through complementary charge-based interactions between the PB region and the high net negative charge of the plasma membrane imparted by the relative abundance of several species of negatively charged lipids (Schmick et al., 2014; Yeung et al., 2008; Zhou et al., 2017).

The 'two signal' model of stable association of peripheral membrane proteins lacking folded lipid binding domains with intracellular membranes also applies to additional members of the Ras family and many other peripheral membrane proteins (Hancock et al., 1989; Heo et al., 2006; Laude and Prior, 2008; Linder et al., 1993; Michaelson et al., 2001). In the absence of a PB region, a second membrane binding module can be provided by an additional lipid anchor, such as the covalent attachment of an acyl group to free cysteine residues. For the farnesylated forms of H-Ras and N-Ras, Golgi localised palmitoyl-acyltransferases (PATs) catalyse the addition of an acyl group to cysteine residues adjacent to the farnesylation motif at the C terminus of H-Ras and N-Ras, trapping these proteins at the Golgi (Hancock et al., 1989; Rocks et al., 2010; Rocks et al., 2005; Swarthout et al., 2005). The opposing action of thioesterase enzymes, such as those of the APT and ABHD families (Anwar and van der Goot, 2023; Won et al., 2018), to remove covalently attached acyl groups helps to prevent the equilibration of S-acylated peripheral membrane proteins across all intracellular membranes

through vesicular transport, concentrating H-Ras and N-Ras at the Golgi and downstream compartments such as the plasma membrane (Dekker et al., 2010; Goodwin et al., 2005; Rocks et al., 2010; Rocks et al., 2005; Salaun et al., 2010).

At present it is unclear how NLRP3 preferentially associates with the Golgi given that only a PB region in NLRP3 has been described (Chen and Chen, 2018). In this study, we went in search of additional signals in NLRP3 that may mediate recruitment of NLRP3 to intracellular membranes alongside the PB region. We find that the Golgi association of NLRP3 is dependent on S-acylation of NLRP3 at a highly conserved cysteine residue (Cys-130) adjacent to the PB region with NLRP3 dynamically associating with the Golgi through reversible S-acylation at Cys-130. Enhanced Golgi recruitment of NLRP3 in response to nigericin is caused by alterations in the NLRP3 S-acylation cycle, which leads to a fraction of NLRP3 becoming immobilised on the Golgi. We show that this immobilisation is attributable to a nigericin induced breakdown in Golgi trafficking, which limits the ability of Golgi resident thioesterase enzymes to encounter NLRP3 and de-acylate it. Our results provide a mechanistic basis for the enhanced Golgi binding observed in response to NLRP3 agonists and suggest that disruptions in organelle homeostasis are coupled to alterations in the NLRP3 S-acylation cycle.

Results

The NLRP3 polybasic region is insufficient to localise NLRP3 to the Golgi

Previous work on NLRP3 has demonstrated that association with TGN46 positive structures is dependent on the NLRP3 polybasic region between residues 131-145. To determine if the NLRP3 polybasic region alone was sufficient to mediate Golgi localisation, we fused the NLRP3 polybasic sequence to GFP (GFP-NLRP3$^{131-158}$) and expressed this construct in HeLaM cells (**Figure 1A**). Expression of GFP-NLRP3$^{131-158}$ was insufficient to achieve a Golgi localisation however and predominantly localised to the nucleus (**Figure 1B - top row, 3rd panel**). As polybasic regions are often paired with a 'second signal' to confer a specific localisation (Heo et al., 2006), we next tested whether the addition of a second membrane binding signal was sufficient to allow association of GFP-NLRP3$^{131-158}$ with intracellular membranes. For this purpose, we appended a C terminal farnesylation motif (CVIM) to GFP-NLRP3$^{131-158}$ (GFP-NLRP3$^{131-158-CVIM}$) (**Figure 1A**). Similar to the charge biosensor probe +8-Pre (Eisenberg et al., 2021; Roy et al., 2000; Yeung et al., 2008), which is farnesylated and contains a PB region with a similar net positive charge to the NLRP3 PB region, expression of GFP-NLRP3$^{131-158-CVIM}$ resulted in strong recruitment of GFP to the plasma membrane (**Figure 1B - middle row, 2nd and 3rd panels, quantified in 1C**). Thus, whilst the PB region alone is insufficient to drive association with intracellular membranes, residues 131-158 within NLRP3 can act in conjunction with a second membrane binding signal to confer binding to specific intracellular membranes.

Identification of additional features necessary for NLRP3 Golgi localisation

Dual membrane binding signals in peripheral membrane proteins are often located near one another in a proteins primary sequence (Hancock et al., 1989; Hancock et al., 1990; Heo et al., 2006). As the PB region alone was insufficient for membrane recruitment, we therefore examined the NLRP3 sequence around the PB region for additional features that may contribute to recruitment of NLRP3 to the Golgi. Two features preceding the NLRP3 polybasic region stand out; a highly conserved cysteine residue at position 130 (Cys-130), which we hypothesised may be S-acylated, and a series of hydrophobic residues upstream of Cys-130 (**Figure 1D**). We speculated that these hydrophobic residues may fulfil an analogous role to the farnesyl anchor in N-Ras and H-Ras, providing a weak non-specific membrane affinity. In a recently published Cryo-EM structure of the inactive NLRP3 complex bound to CRID3 (Hochheiser et al., 2022), the hydrophobic residues form part an alpha helix (residues 115-125, helix$^{115-125}$), with several hydrophobic residues (I113, W117, L120, L121, L24) aligned along a single face (**Figure 1D, E**). Cys-130 resides between helix$^{115-125}$ and the polybasic

region. Helix[115-125] and Cys-130 sit at the centre of one NLRP3 pentamer and are largely surface exposed, as they face away from the core of the decameric complex (**Supplementary Figure 1A**), suggesting these additional features may work together with the polybasic region to allow localisation to the Golgi.

To first determine if NLRP3 Golgi association was dependent on S-acylation, we treated cells with 2-bromopalmitate (2-BP), a palmitic acid analogue which is thought to block global protein S-acylation through covalent binding to the active site of ZDHHC enzymes (Davda et al., 2013; Jennings et al., 2009; Webb et al., 2000). Golgi enrichment of NLRP3 in HeLaM cells transiently transfected with GFP-tagged NLRP3 was inhibited by treatment of cells with 2-BP (**Figure 1F, G**), suggesting that S-acylation regulates recruitment of NLRP3 to the Golgi. Several studies have demonstrated that NLRP3 stimuli cause an increase in the recruitment of NLRP3 to the Golgi (Chen and Chen, 2018; Lee et al., 2023; Schmacke et al., 2022) which

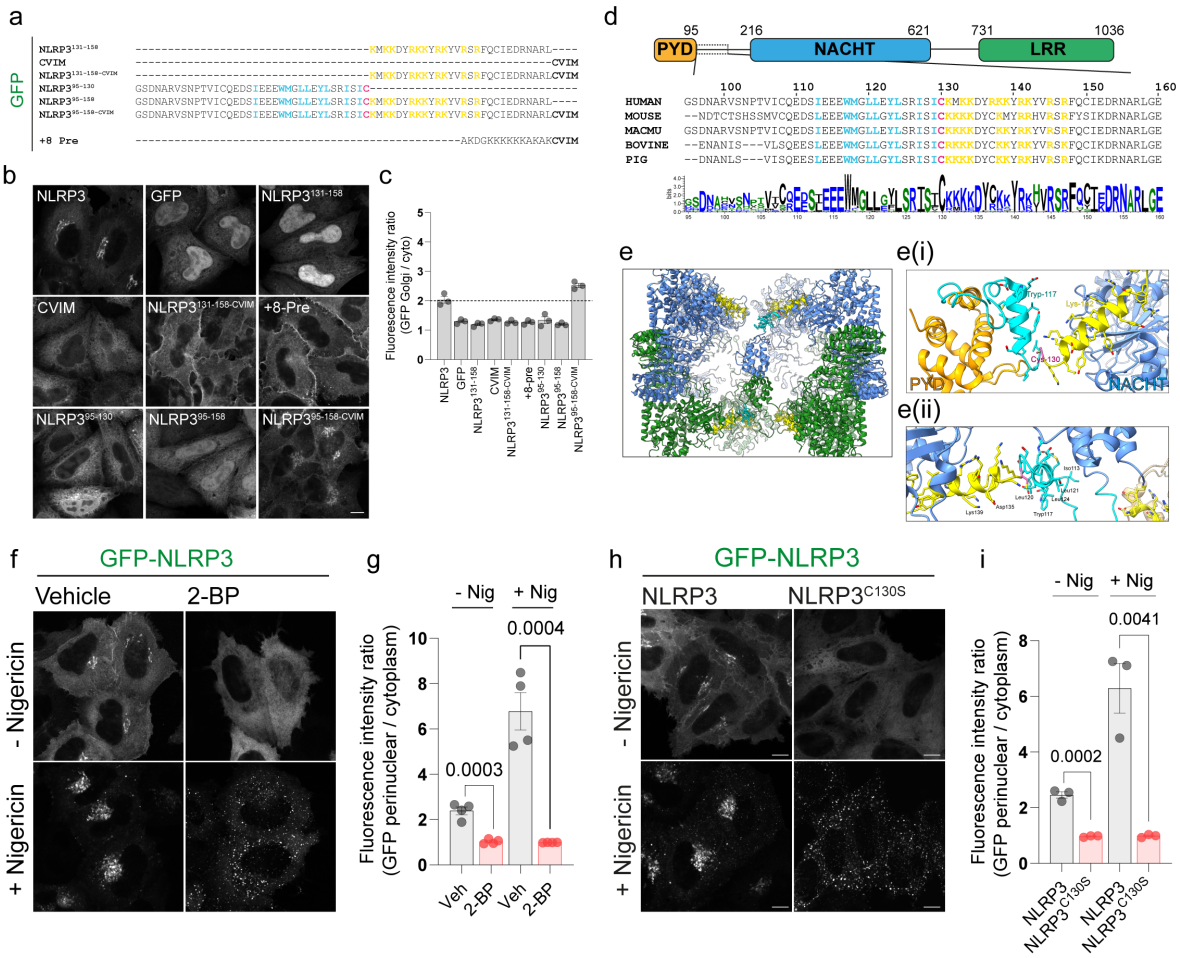

Figure 1. Association of NLRP3 with intracellular membranes is dependent on S-acylation. A) Schematic of the sequences used for GFP tagged minimal NLRP3 constructs expressed transiently in HeLaM cells. **B)** Representative confocal microscopy images of each construct expressed. Scale bar = 10 µm. **C)** Quantification of the amount of each mini-construct localised to the Golgi relative to cytosolic signal. N=3. **D)** Overview of domain architecture of NLRP3. Boxed region indicates region and residues shown below with sequence conservation across 20 species represented by a web-logo plot. **E)** ChimeraX graphic based on the inactive Cryo-EM structure of NLRP3 (PDB ID: 7PZC) showing a side view of the NLRP3 decamer. Monomers within each pentamer are colour coded blue or green. One monomer from each pentamer is hidden to give a clearer view of helix[115-125] (coloured cyan with Cys-130 in pink) and the polybasic region from each monomer (coloured yellow). **Ei)** Graphic showing the position of residues 95-146 relative to the PYD and NACHT domains. **Eii)** Zoom in looking along helix[115-125]. Residues Tryp117, Leu120, Leu121 and Leu124 (labelled) align along a single face of helix[115-125]. **F)** Representative confocal microscopy images of HeLaM cells transiently expressing GFP-NLRP3 treated with either 0.5% DMSO or 100 µM 2-BP for 16 hours with or without a 1-hour treatment with 10 µM nigericin and **G)** quantification of GFP-NLRP3 signal associated with the Golgi from the same experiment. N = 4. Scale bar = 10 µm. **H)** Representative images of HeLaM cells transiently expressing GFP-NLRP3 or GFP-NLRP3[C130S] treated with

or without 10 μM nigericin for 1 hour. Scale bar = 10 μm. **I)** Quantification of GFP-NLRP3 or GFP-NLRP3^{C130S} on the Golgi before and after nigericin treatment. N = 4

we also observed here following nigericin treatment (**Figure 1F, G, Supplementary Figure 2A, B, C**). To test whether this enhanced recruitment was dependent on S-acylation we pre-treated cells with 2-BP overnight prior to a 1-hour stimulation with nigericin. 2-BP treatment prevented the perinuclear clustering of NLRP3 signal observed following nigericin stimulation and instead induced the formation of peripherally localised aggregates (**Figure 1F, G**), indicating that enhanced recruitment of NLRP3 to the perinuclear region in response to NLRP3 stimuli is S-acylation dependent. In agreement with Cys-130 being a critical determinant of NLRP3 Golgi localisation, mutation of this residue phenocopied the effect of 2-BP, preventing Golgi enrichment of GFP-NLRP3 at steady state and in response to nigericin treatment (**Figure 1H, I**). The sensitivity of NLRP3 membrane binding to 2-BP and mutation of Cys-130 could also be seen with an untagged NLRP3 construct, although NLRP3^{C130S} did not form peripheral puncta in response to nigericin, suggesting these may be an artifact of GFP tagging (**Supplementary Figure 3A**). To test whether the hydrophobic residues within helix$^{115-125}$ are also important for membrane binding we mutated residues isoleucine-113, tryptophan-117, leucine-120 and leucine-124 (hydrophobic face mutant; NLRP3^{HF}), which are predicted to form a hydrophobic face as part of helix$^{115-125}$ (**Supplementary Figure 4A, B**). These mutations abolished recruitment of NLRP3 to the Golgi at steady state and in response to nigericin (**Supplementary Figure 4C**), indicating that these residues also play an important role in recruitment of NLRP3 to intracellular membranes alongside Cys-130 and the polybasic region.

Definition of a minimal NLRP3 membrane binding region

To determine if Cys-130 and helix$^{115-125}$ were sufficient in isolation to drive Golgi localisation, we again expressed minimal NLRP3 peptides containing these residues in cells. GFP alone localised to both the nucleus and cytoplasm (**Figure 1B, top row, 1st panel**). In contrast, expression of GFP-NLRP3-95-130 (NLRP3$^{95-130}$), containing both helix$^{115-125}$ and Cys-130, localised predominantly to the cytoplasm with some Golgi enrichment visible, however this was not at levels similar to full length NLRP3 (**Figure 1B – bottom row, 1st panel**). Surprisingly, inclusion of the polybasic region in the minimal peptide (residues 95-158) also failed to recapitulate Golgi enrichment equivalent to the full-length protein (**Figure 1B – bottom row, 2nd panel**), suggesting that additional features within NLRP3 are necessary to achieve recruitment to the Golgi. To define a minimal NLRP3 region that shows levels of Golgi enrichment equivalent to the full-length protein, we created NLRP3 mutants truncated from either the N or C terminus. Removal of the pyrin domain (PYD, residues 1-95) had no impact on Golgi localisation, however further truncation to residue 121 abolished NLRP3's Golgi localisation, consistent with the requirement for helix$^{115-125}$ (**Supplementary Figure 5A-C, H**). A minimal C terminal NLRP3 truncation to residue 699 was found to be sufficient for Golgi localisation with further truncation down to residue 680 abolishing NLRP3 Golgi enrichment (**Supplementary Figure 5D-F, H**). Based on these results, we expressed a minimal NLRP3 construct spanning residues 95-699. This construct displayed variable levels of Golgi localisation in untreated cells and had a noticeably weaker response to nigericin (**Supplementary Figure 5G-H**) suggesting that the PYD and LRR may have additive effects which facilitate Golgi binding, potentially through stabilisation of the NLRP3 cage (Andreeva et al., 2021; Hochheiser et al., 2022). Consistent with the need for an additional membrane affinity to drive Golgi enrichment of NLRP3, attachment of C-terminal farnesylation sequence (CVIM) to residues 95-158 was sufficient to achieve levels of Cys-130 dependent Golgi enrichment comparable to full length NLRP3 (**Figure 1B, bottom row, 3rd panel, quantified in 1C**) with this construct also showing a high degree of overlap with untagged NLRP3 at the Golgi (**Supplementary Figure 6A-E**). Thus, whilst helix$^{115-125}$, Cys-130 and the polybasic region are all essential for Golgi localisation, additional properties in NLRP3 are required to allow full Golgi binding.

ZDHHC3 and ZDHHC7 overexpression enhance the Golgi localisation of NLRP3

Protein S-acylation is mediated by a family of 23 palmitoyltransferases (PAT) in humans (Lemonidis et al., 2015). PATs are multi-pass transmembrane proteins defined by the presence of a characteristic zinc dependent DHHC domain (zDHHC) responsible for the covalent attachment of acyl chains of varying length to exposed cysteine residues on target substrates (Fukata et al., 2004; Greaves et al., 2017; Jennings and Linder, 2012; Ohno et al., 2006). To probe whether the Golgi localisation of NLRP3 is sensitive to ZDHHC overexpression, indicative of NLRP3 membrane binding being controlled by S-acylation, we co-expressed a library of HA-tagged ZDHHC enzymes alongside GFP-NLRP3. Overexpression of the related enzymes ZDHHC3 and ZDHHC7 both markedly enhanced recruitment of NLRP3 to the Golgi at the expense of cytosolic NLRP3 signal, with ZDHHC3 having a slightly stronger effect than ZDHHC7 (**Figure 2A, B**). To a much weaker extent, ZDHHC2, ZDHHC8 and ZDHHC9 also enhanced NLRP3 Golgi recruitment (**Figure 2A**). Unexpectedly, overexpression of the plasma membrane localised PAT ZDHHC5 decreased the amount of NLRP3 at the Golgi and instead caused NLRP3 to re-localise to the plasma membrane (**Figure 2A, B**).

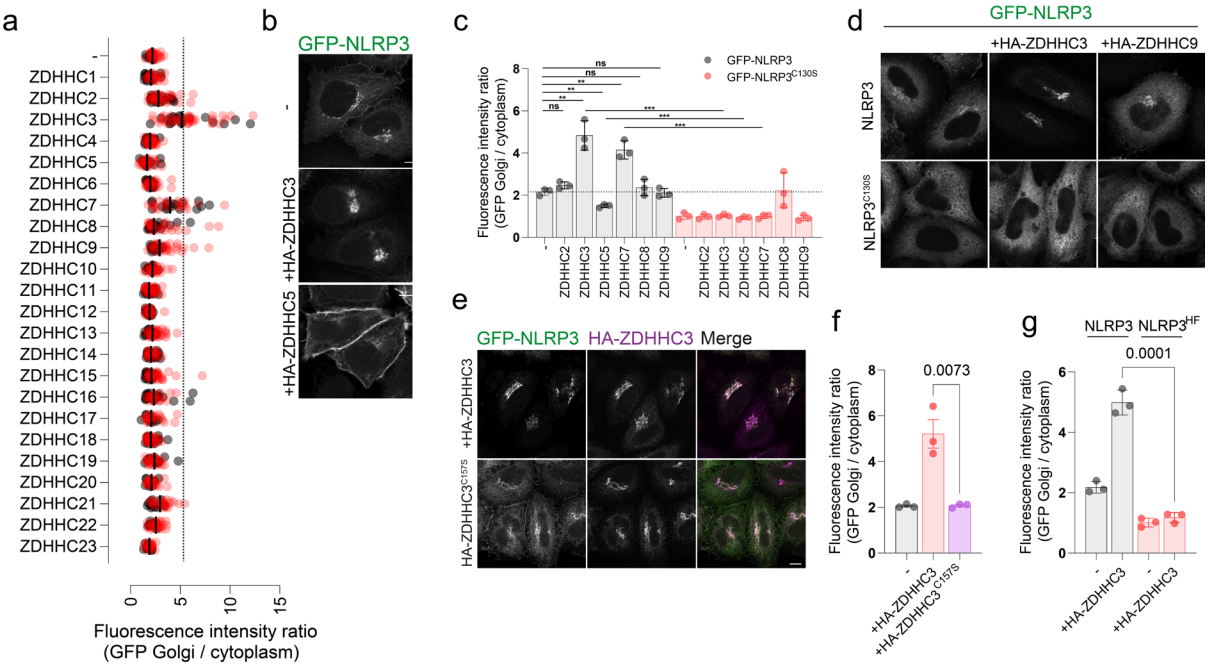

Figure 2. Overexpression of ZDHHC palmitoyltransferases can alter NLRP3 localisation in a Cys-130 and helix$^{115-125}$ dependent manner. A) Quantification of the ratio of GFP-NLRP3 signal on the Golgi relative to that in the cytosol in HeLaM cells transiently transfected with 1 µg of each individual HA-tagged ZDHHC enzyme and GFP-NLRP3. N = 2. **B)** Representative confocal microscopy images showing the effect of HA-ZDHHC3 and HA-ZDHHC5 on the localisation of GFP-NLRP3. Scale bars = 10 µm. **C)** Quantification of GFP-NLRP3 or GFP-NLRP3^{C130S} Golgi signal in HeLaM cells transiently transfected with lower amounts (0.25 µg) of each HA-ZDHHC enzyme which altered GFP-NLRP3 localisation in (A). N = 3. **p < 0.01, ***p < 0.001 (Unpaired t test). **D)** Representative confocal microscopy images of GFP-NLRP3 or GFP-NLRP3^{C130S} expressed with the indicated HA tagged ZDHHC enzyme. HA-ZDHHC9 images demonstrate that not all Golgi localised PATs drive enhanced Golgi recruitment of NLRP3. **E)** Representative confocal microscopy images of GFP-NLRP3 Golgi recruitment in cells transfected with wild type HA-ZDHHC3 or catalytically inactive HA-ZDHHC3^{C157S}. Scale bar = 10 µm. **F)** Quantification of GFP-NLRP3 Golgi signal in HeLaM cells co-transfected with HA-ZDHHC3 and catalytically inactive HA-ZDHHC3^{C157S}. N = 3. **G)** Quantification of GFP-NLRP3 or GFP-NLRP3^{HF} signal on the Golgi in HeLaM cells transiently transfected with 0.25 µg HA-ZDHHC3. N = 3.

In a secondary screen using lower amounts of each ZDHHC enzyme, ZDHHC3, ZDHHC5 and ZDHHC7 all altered NLRP3 localisation to a similar degree seen when using higher amounts of DNA, however ZDHHC2, ZDHHC8 and ZDHHC9 had minimal impact on Golgi recruitment when expressed at lower levels (**Figure 2C, D**). Consistent with the results seen for GFP-tagged NLRP3, ZDHHC3 and ZDHHC5 also altered the localisation of untagged NLRP3 (**Supplementary Figure 3B**). The effect of ZDHHC overexpression on NLRP3 localisation

242 was dependent on the catalytic activity of the enzyme as catalytically inactive ZDHHC3^{C157S}
243 had no effect on recruitment on NLRP3 to the Golgi (**Figure 2E, F**). Thus, the localisation of
244 NLRP3 can be altered by manipulating the levels and activity of ZDHHC enzymes, consistent
245 with S-acylation controlling the sub-cellular localisation of NLRP3. Cys-130 and hydrophobic
246 residues within helix$^{115-125}$ were both essential for the enhanced effect of ZDHHC3 and
247 ZDHHC7 on NLRP3 Golgi recruitment and the effect of ZDHHC5 on recruitment of NLRP3 to
248 the plasma membrane as mutating either of these features prevented NLRP3 re-localisation
249 in response to ZDHHC overexpression (**Figure 2C, G, Supplementary Figure 3B-C,**
250 **Supplementary Figure 4D**).

251 To gain further insight into how helix$^{115-125}$ and Cys-130 act together with the PB region to drive
252 interaction of NLRP3 with intracellular membranes, we co-expressed NLRP3 containing
253 mutations in the polybasic region with ZDHHC3 or ZDHHC5. PB mutations prevented
254 localisation of NLRP3 to the Golgi at steady state and in response to nigericin, consistent with
255 previous reports (**Supplementary Figure 7A**) (Chen and Chen, 2018). In agreement with the
256 polybasic region driving affinity for highly charged membranes such as the plasma membrane
257 and TGN (Eisenberg et al., 2021), sensitivity to PM localised ZDHHC5 required an intact PB
258 region (**Supplementary Figure 7B**), however cis-Golgi localised ZDHHC3 (Ernst et al., 2018)
259 was still able to recruit NLRP3 when the PB region was mutated (**Supplementary Figure 7C,**
260 **D**). These results suggest that helix$^{115-125}$ and Cys-130 can drive low levels of interaction with
261 intracellular membranes independent of the polybasic region, likely through the hydrophobic
262 residues within helix$^{115-125}$, but not at sufficient levels to show noticeable enrichment. The
263 presence of the PB region works synergistically with helix$^{115-125}$ to boost membrane affinity,
264 preferentially favouring membranes with a high net negative charge, as illustrated by PB
265 dependent plasma membrane trapping in the presence of overexpressed HA-ZDHHC5.

266 **NLRP3 Localisation to the Golgi in macrophages is dependent on Cys-130 and helix^{115-}**
267 **^{125}**

268 As NLRP3 is predominantly expressed in myeloid cell types such as macrophages and
269 monocytes, we stably transduced THP-1 cells with GFP-NLRP3, GFP-NLRP3^{C130S} or GFP-
270 NLRP3^{HF} and assessed Golgi localisation in PMA treated THP-1 cells to determine whether
271 Cys-130 and helix$^{115-125}$ are also required for localisation to the Golgi in macrophages. As
272 previously described (Andreeva et al., 2021; Chen and Chen, 2018), endogenous NLRP3
273 localised to the perinuclear region where it partially overlapped with the *trans*-Golgi marker
274 p230 (**Figure 3A**), with this perinuclear localisation matched by GFP-NLRP3 (**Figure 3B**).
275 Consistent with the requirement for Cys-130 and the preceding hydrophobic residues for Golgi
276 localisation in HeLaM cells, mutation of these residues removed the perinuclear pool of NLRP3
277 (**Figure 3B, C**), with GFP-NLRP3 also sensitive to overexpression of HA-tagged ZDHHC3 in
278 a manner that was again dependent on Cys-130 (**Figure 3D**). To test the effects of enhanced
279 levels of ZDHHC3 activity on inflammasome activation, we measured levels of nigericin
280 induced cell death by propidium iodide (PI) staining of cells stably expressing HA-tagged
281 ZDHHC3, as this had the strongest effect on NLRP3 Golgi recruitment in both HeLaM cells
282 and THP-1 cells. Wild type but not catalytically inactive HA-ZDHHC3^{C157S} enhanced Golgi
283 recruitment of endogenous NLRP3 (**Figure 3E**) and markedly enhanced the percentage of
284 cells positive for PI following nigericin treatment (**Figure 3F, G**), suggesting that higher levels
285 of ZDHHC3 activity can induce a greater percentage of cells to undergo NLRP3 dependent
286 cell death.

287 **NLRP3 can be S-acylated at Cys-130**

288 To determine if the cysteine at position 130 is S-acylated, we visualised NLRP3 S-acylation
289 using an acyl-biotin exchange (ABE) assay and 5kDa PEG maleimide, which adds an
290 additional mass of 5kDa to every cysteine residue that is S-acylated. Recent work has shown
291 that NLRP3 is S-acylated within its LRR domain at position 844 by the Golgi localised PAT

ZDHHC12 (Wang et al., 2023) and at Cys-8 within the PYD domain (Lv et al., 2023). S-acylation at Cys-8 and Cys-844 are both dispensable for recruitment to the Golgi as deletion of the PYD or LRR domains had minimal effect on Golgi recruitment (**Supplementary Figure 5**). Consistent with the presence of multiple cysteines in NLRP3 being S-acylated, labelling of S-acylated cysteines in NLRP3 revealed two bands indicative of singly and doubly S-acylated NLRP3 species in both HeLaM and THP1 cells (**Figure 4A, C**). A large amount of NLRP3 remained resistant to hydroxylamine, suggesting a significant proportion of NLRP3 is not S-acylated at steady state. Surprisingly, mutation of Cys-130 led to only subtle changes in the S-acylation profile of NLRP3 with no loss of doubly S-acylated NLRP3 (**Figure 4A, C**), suggesting this species may represent a mix of S-acylation events at dual cysteines (i.e. Cys8/Cys844, Cys8/Cys130, Cys130/Cys844). The absence of a third band (Cys8, Cys130, Cys844) also suggests that S-acylation events at Cys-8, Cys-130 and Cys-844 may be mutually exclusive. Enhanced NLRP3 Golgi binding driven by ZDHHC3 over-expression and nigericin treatment both correlated with an increased amount of a singly S-acylated wild type NLRP3 species which did not occur when Cys-130 was mutated (**Figure 4A, B**).

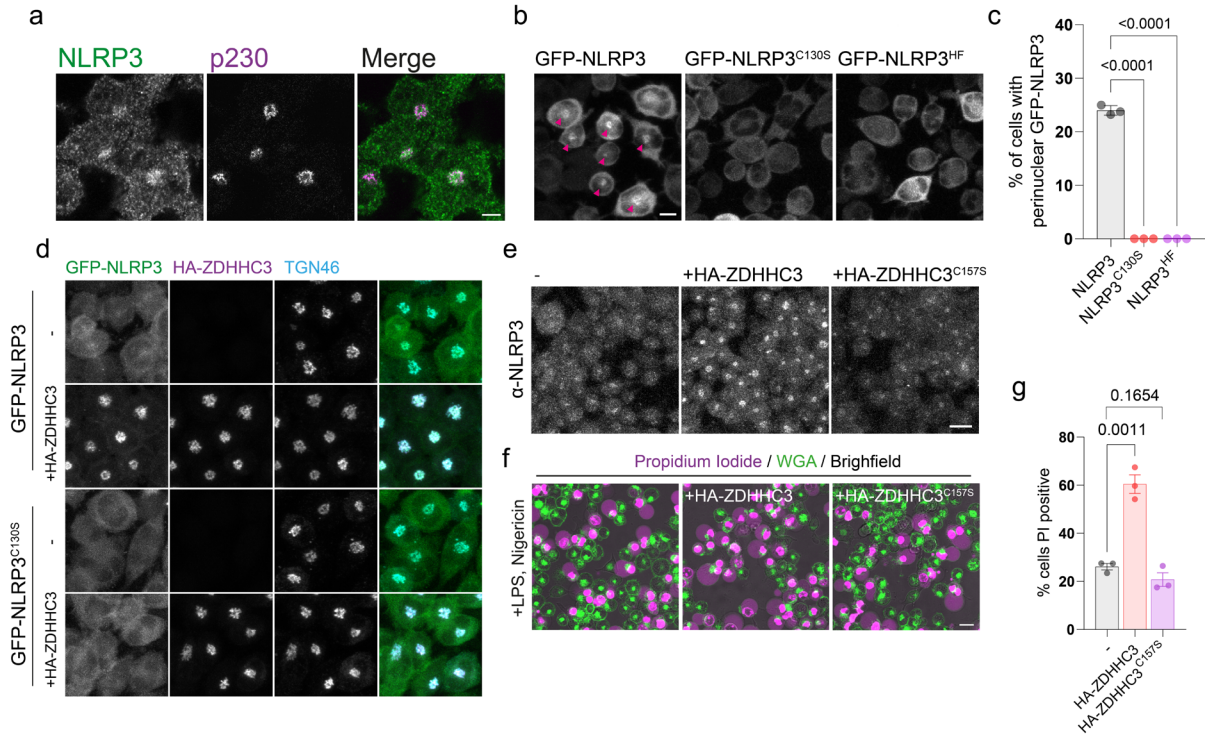

Figure 3. NLRP3 localisation to the Golgi is Cys-130 dependent and sensitive to ZDHHC3 levels in THP-1 macrophages. A) Confocal microscopy images of LPS stimulated THP-1 cells stained with antibodies against NLRP3 and p230. Scale bar = 5 µm. **B)** THP-1 cells stably transduced with either GFP-NLRP3, GFP-NLRP3^{C130S}, or GFP-NLRP3^{HF} were imaged live by confocal microscopy and scored in **C)** for the percentage of cells showing a perinuclear enrichment of GFP-NLRP3 signal. N = 3. Scale bar = 10 µm. **D)** Confocal microscopy images of stable GFP-NLRP3 or GFP-NLRP3^{C130S} THP-1 cells transduced with HA-ZDHHC3 and stained for HA to visualise ZDHHC3 localisation and TGN46. Images are representative of two independent experiments. **E)** THP-1 cells stably over-expressing HA-ZDHHC3 or HA-ZDHHC3^{C157S} were stained with anti-NLRP3 antibodies to visualise NLRP3 recruitment to the peri-nuclear region. Scale bar = 20 µm. **F)** Representative live cell confocal microscopy images of LPS primed THP-1 cells stably over-expressing HA-ZDHHC3 or HA-ZDHHC3^{C157S} stimulated with 20 µM nigericin for 2 hours. Dead cells were visualised by propidium iodide staining with cell boundaries visualised through WGA-Alexa647 staining. Scale bar = 20 µm. **G)** Quantification of the percentage of non-transduced, HA-ZDHHC3 or HA-ZDHHC3^{C157S} THP-1 cells positive for propidium iodide following treatment with 20 µM nigericin for 2 hours. N = 3.

As efforts to determine whether NLRP3 is S-acylated at Cys-130 were complicated by the presence of additional S-acylation sites in NLRP3, we next attempted to confirm S-acylation at Cys-130 using GFP-NLRP3$^{95-158}$, which incorporates helix$^{115-125}$, Cys-130 and the PB region (**Figure 4D**). GFP-NLRP3$^{95-158}$ displayed no mass shift following labelling of exposed S-

acylated cysteine and did not localise to the Golgi (**Figure 4E-G**), indicating that in the context of the small peptide used for this experiment, Cys-130 is not significantly S-acylated at steady state. However, overexpression of HA-ZDHHC3 significantly increased enrichment of NLRP3$^{95\text{-}158}$ at the Golgi (**Figure 4E, F**) and induced a mass shift of NLRP3$^{95\text{-}158}$ following 5kDa PEG maleimide labelling that was dependent on Cys-130 and the preceding hydrophobic residues (**Figure 4G**). These results provide evidence that the linker region preceding the PB region is capable of undergoing S-acylation at Cys-130. Similar to their full-length counterparts (**Supplementary Figure 7B, C**), NLRP3$^{95\text{-}158}$ peptides containing mutations in the PB region remained as sensitive to HA-ZDHHC3 overexpression as WT NLRP3 (**Supplementary Figure 7E-H**).

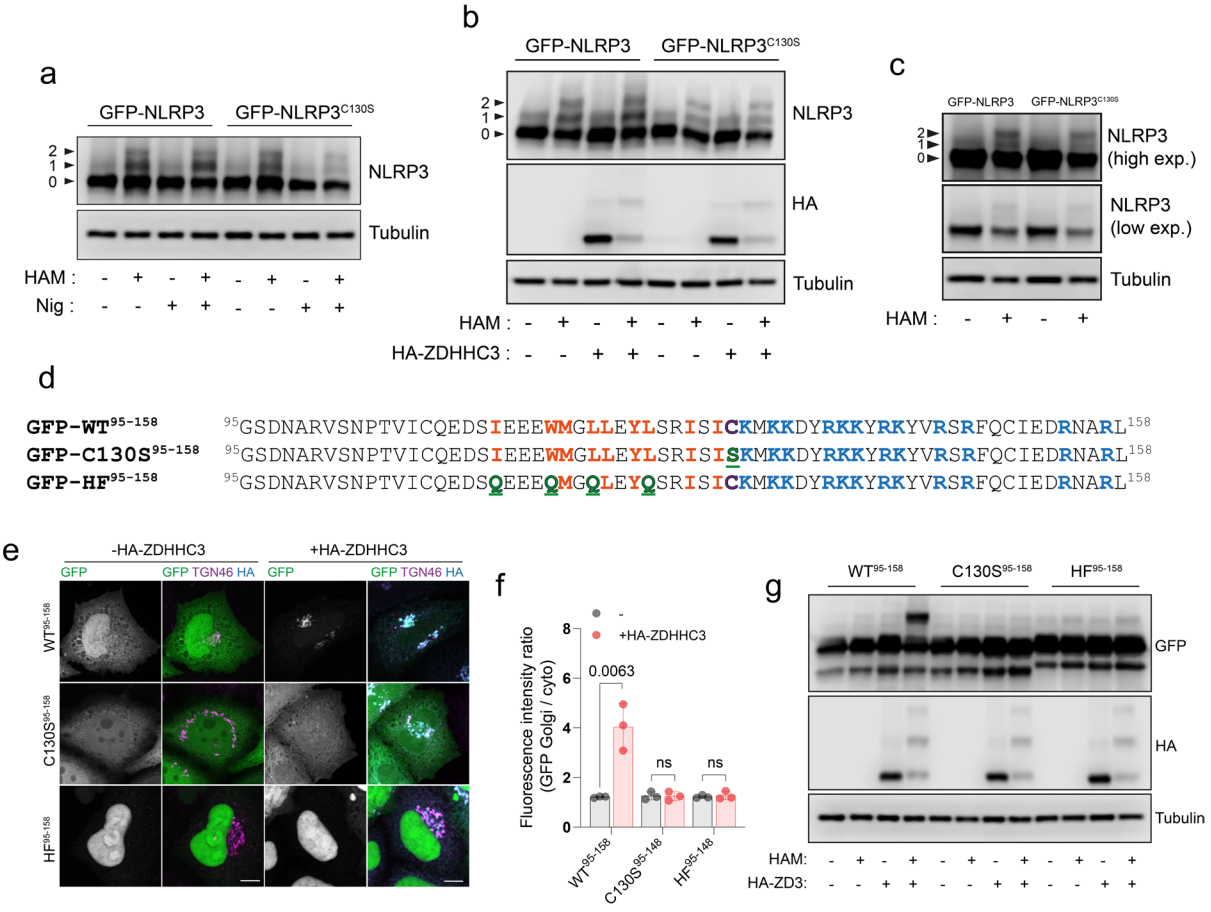

Figure 4. NLRP3 can be S-acylated at Cys-130. A) Visualisation of S-acylation sites in HeLaM cells transiently expressing GFP-NLRP3 or GFP-NLRP3^{C130S}, labelled by an acyl biotin exchange assay (ABE) with 5-kDa PEG maleimide. Arrowheads indicate non-lipidated NLRP3 (0), singly S-acylated NLRP3 (1) and doubly acylated NLRP3 (2) species. **B)** Visualisation of acylation sites by 5kDa PEG maleimide ABE in HeLaM cells transiently expressing GFP-NLRP3 or GFP-NLRP3^{C130S} and 0.25 µg HA-ZDHHC3. **C)** Visualisation of acylation sites by 5kDa PEG maleimide ABE in THP-1 cells stably transduced with GFP-NLRP3 or GFP-NLRP3^{C130S}. Blots are representative of 2 independent experiments. **D)** Schematic of minimal GFP tagged NLRP3 sequences used and expressed in HeLaM cells to directly assess S-acylation at Cys-130. Mutations introduced are highlighted in green. **E)** Representative confocal microscopy images of GFP-NLRP3$^{95\text{-}158}$, GFP-NLRP3$^{C130S,95\text{-}158}$ or GFP-NLRP3$^{HF,95\text{-}158}$, expressed alone or with 0.25 µg HA-ZDHHC3. N = 3. Scale bars = 10 µm. **F)** Quantification of GFP-NLRP3$^{95\text{-}158}$, GFP-NLRP3$^{C130S,95\text{-}158}$ or GFP-NLRP3$^{HF,95\text{-}158}$ signal associated with the Golgi with or without HA-ZDHHC3. **G)** Visualization of S-acylation sites in GFP-NLRP3$^{95\text{-}158}$ peptides expressed in HeLaM cells by ABE with or without 0.25 µg HA-ZDHHC3.

NLRP3 is concentrated at the Golgi by an S-acylation cycle

S-acylation of proteins can be reversed by the action of the APT and ABHD family of thioesterases which catalyse the removal of acyl groups from S-acylated cysteine residues (Lin and Conibear, 2015; Tomatis et al., 2010; Won et al., 2018). Small molecule inhibition of

thioesterase activity by the Palmostatin family of compounds has been shown to abolish the TGN and PM localisation of H-Ras and N-Ras and leads to their redistribution across intracellular membranes (Dekker et al., 2010) due the stability of membrane binding provided by an acyl lipid anchor and carry over of acylated Ras proteins to the PM on vesicular carriers (Apolloni et al., 2000). Treatment of cells expressing GFP-NLRP3 with PalmostatinB had a similar effect on NLRP3, with loss of NLRP3 signal at the Golgi (**Figure 5A**) and re-localisation of NLRP3 to the plasma membrane, tubular recycling endosomes, and late endosomes (**Supplementary Figure 8A, B, C**). Consistent with NLRP3 undergoing de-acylation, overexpression of the Golgi localised thioesterase APT2 (Abrami et al., 2021), but not mitochondrially localised APT1 (Kathayat et al., 2018), significantly reduced localisation of NLRP3 to the Golgi in unstimulated cells (**Figure 5B**). Both PalmostatinB treatment and APT2 overexpression also limited the accumulation of NLRP3 on the Golgi in response to nigericin (**Figure 5C, D**), although likely for different reasons; NLRP3 remains membrane bound following PalmostatinB treatment but is physically segregated from the Golgi on post-Golgi compartments, whilst APT2 overexpression likely acts to block significant accumulation of NLRP3 on the Golgi through higher rates of NLRP3 de-acylation. The effect of APT2

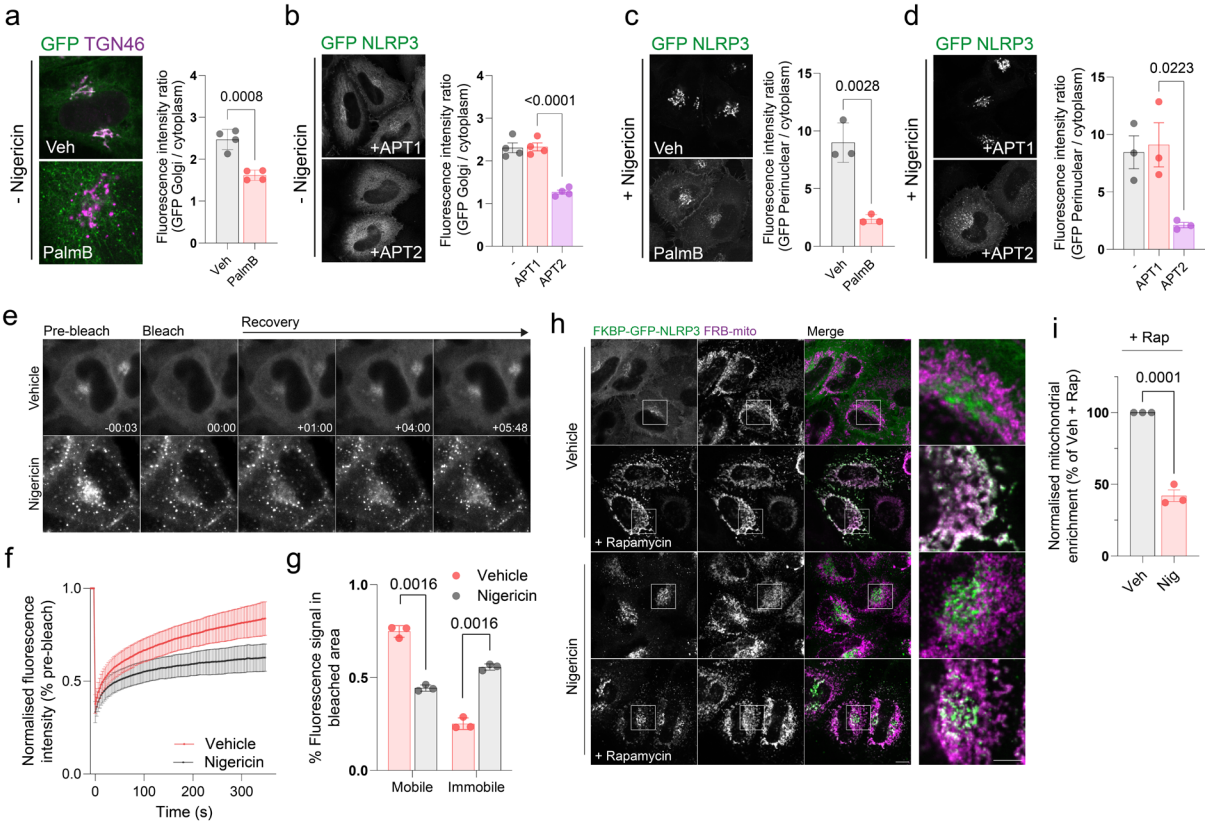

Figure 5. NLRP3 dynamically associates with the Golgi apparatus. A) Representative confocal microscopy images of GFP-NLRP3 relative to TGN46 in cells treated for 4 hours with 50 µM PalmostatinB or 0.4% DMSO vehicle control and quantification of GFP-NLRP3 signal associated with the Golgi with or without PalmostatinB treatment. **B)** Representative images of GFP-NLRP3 in HeLaM cells co-expressed with 0.25 µg APT1-FLAG or 0.25 µg APT2-FLAG with quantification of GFP-NLRP3 signal associated with the Golgi in cells overexpressing APT1-FLAG or APT2-FLAG. Golgi associated GFP-NLRP3 signal is lost in cells expressing APT2-FLAG. **C)** Representative confocal images of the effect of PalmostatinB treatment on enhanced recruitment of NLRP3 to the Golgi after nigericin treatment and quantification of perinuclear GFP-NLRP3 signal. Cells were pre-treated for 4 hours with 50 µM PalmostatinB or 0.4% DMSO control before a 1-hour stimulation with 10 µM nigericin. **D)** Representative microscopy images of GFP-NLRP3 and APT1 or APT2-FLAG expressing cells following a 1 hour treatment with 10 µM nigericin and quantification of GFP-NLRP3 signal on the Golgi under the same conditions. **E)** Representative images of GFP-NLRP3 expressing HeLaM cells before and after photobleaching of Golgi associated NLRP3. **F)** FRAP recovery curves of GFP-NLRP3 transiently expressed in HeLaM cells treated with vehicle control or 10 µM nigericin for 1 hour. **G)** Quantification of the mobile and immobile pool of GFP-NLRP3 signal in cells treated with vehicle control or 10 µM nigericin. **H)** Representative confocal microscopy images of

mitochondrial re-routing of FKBP tagged GFP-NLRP3 transiently expressed in HeLaM cells. Cells were treated with either vehicle control or 10 μM nigericin for 1 hour before a 15-minute co-incubation with 500 nM rapamycin prior to fixation. Scale bars in main figure = 10 μm, insets 5 μm. **I)** Quantification of the amount of GFP-NLRP3 signal associated with the mitochondria following rapamycin treatment in the presence of absence of nigericin. Values are expressed as a percentage of the mitochondrial to cytosolic GFP-NLRP3 ratio seen in vehicle treated control cells.

overexpression appeared to be acute, suggestive of a direct action on NLRP3, as mitochondrial re-routing of APT2 from the Golgi prior to nigericin stimulation restored the enhanced recruitment of NLRP3 to the Golgi observed in response to nigericin (**Supplementary Figure 9A-F**). Thus, NLRP3 dynamically associates with intracellular membranes through an S-acylation cycle.

Nigericin treatment immobilises NLRP3 on Golgi membranes

The amount of NLRP3 recruited to the Golgi increases following NLRP3 activation (**Supplementary Figure 2A-C**) (Chen and Chen, 2018), with this process proposed to represent a response to a danger signal common to multiple NLRP3 stimuli. The basis for enhanced Golgi recruitment is unknown. To test whether the membrane binding cycle of NLRP3 is altered in response to nigericin, we monitored the dynamics of NLRP3 membrane association by performing fluorescence recovery after photobleaching (FRAP) experiments on GFP-NLRP3 in the presence or absence of nigericin. The kinetics of NLRP3 membrane binding in untreated cells were similar to those described for mono-S-acylated N-Ras (Rocks et al., 2005) with a half time to recovery of 58.4 seconds (± 9.3 seconds S.D.), in agreement with NLRP3 rapidly cycling on and off the Golgi in an S-acylation cycle (**Figure 5E, F**). Nigericin treatment suppressed the fluorescence recovery; whilst GFP-NLRP3 signal on average recovered to 75% of the pre-bleach signal in untreated cells, this was reduced to 44% after nigericin treatment, indicating that a greater fraction of NLRP3 that makes up the signal in the Golgi region is immobile following nigericin treatment (**Figure 5G**). Reduced mobility of Golgi localised NLRP3 by FRAP was consistent with a mitochondrial re-routing assay using FKBP tagged GFP-NLRP3 where a proportion of perinuclear NLRP3 in nigericin treated cells remained resistant to rapamycin induced mitochondrial re-routing (**Figure 5H, I**). Changes in the membrane binding cycle of NLRP3 therefore accompany its activation, with less NLRP3 cycling off Golgi membranes following nigericin treatment.

Immobilisation of NLRP3 on the Golgi is due to segregation from de-acylating enzymes

We next sought to understand how NLRP3 becomes immobilised on the Golgi. Golgi binding in nigericin treated cells is dependent on S-acylation at Cys-130 (**Figure 1H, I**), suggesting that increased Golgi recruitment of NLRP3 could potentially be a result of changes in the Cys-130 S-acylation cycle, either through higher rates of S-acylation or lower rates of de-acylation. As a fraction of NLRP3 was resistant to mitochondrial rerouting (**Figure 5H, I**), suggestive of less NLRP3 being de-acylated, we tested whether immobilisation of NLRP3 may be the result of changes in the access of thioresterase enzymes to NLRP3 post nigericin treatment. The thioesterase enzyme APT2 is known to reside at the Golgi and is tethered to its cytoplasmic face by S-acylation (Abrami et al., 2021; Anwar and van der Goot, 2023; Lin and Conibear, 2015; Vartak et al., 2014). APT2 is S-acylated by the *cis*-Golgi localised PATs ZDHHC3 and ZDHHC7 (Abrami et al., 2021; Ernst et al., 2018), suggesting APT2 is predominantly S-acylated at the cis-Golgi with access to the medial and trans Golgi likely in part requiring anterograde trafficking between Golgi cisternae to remain intact. To examine overlap between APT2 and NLRP3, we used the catalytically inactive APT2 mutant APT2^{S122A} (Toyoda et al., 1999; Wang et al., 1997) to prevent overexpressed APT2 from clearing NLRP3 from the Golgi. In untreated cells, APT2^{S122A} and NLRP3 signal were closely opposed (**Figure 6A, B**). However, whilst some NLRP3 signal overlapped with APT2^{S122A} after nigericin treatment, a large proportion of NLRP3 accumulated on structures that were largely devoid of APT2^{S122A} (**Figure 6A, B**) indicating that APT2 becomes segregated from NLRP3 following nigericin treatment.

To test whether segregation between NLRP3 and APT2 after nigericin treatment was due to impaired trafficking through the Golgi, we monitored Golgi function with a secretory reporter system that utilises a modified version of human growth hormone (EGFP-FM4-hGH, hereafter referred to as FM4-hGH), a luminal cargo which is normally secreted from cells via the Golgi. In this system, hGH is tagged to four repeats of FKBP containing an F>M mutation at position 36 (Rollins et al., 2000). This mutation causes FKBP to aggregate and leads to retention of FKBP tagged hGH in the lumen of the ER (Gordon et al., 2010; Rivera et al., 2000). FM4-hGH aggregates can be solubilised by the addition of rapamycin, which allows FM4-hGH to then be exported from the ER and transit through the Golgi stack before being secreted (**Figure 6C**). Nigericin treatment in the presence of rapamycin had no effect on exit of FM4-hGH from the ER, but inhibited its trafficking through the Golgi, with FM4-hGH accumulating in structures which overlapped with the *cis*-Golgi marker STX5 (**Figure 6D, E**), suggesting that the flow of material beyond *cis* and *medial* Golgi cisternae is impaired by nigericin. Consistent with segregation of NLRP3 from earlier Golgi compartments, minimal overlap of STX5 and hGH with NLRP3 could be seen following nigericin treatment (**Supplementary Figure 10A-D**). Thus, impaired trafficking through the Golgi limits the ability of APT2 to come into contact with NLRP3 and de-acylate it, which likely underpins the gradual accumulation of NLRP3 on the Golgi seen following nigericin treatment (**Figure 6F,G**). Enhanced Golgi recruitment of NLRP3 appears to be insufficient for NLRP3 activation however as treatment of cells with the Na^+ selective ionophore monensin, which does not activate NLRP3 (Munoz-Planillo et al., 2013; Perregaux et al., 1992), also induced an accumulation of NLRP3 on Golgi membranes (**Supplementary Figure 11A, B, C**) that was concomitant with a block in Golgi trafficking (**Supplementary 11D, E**).

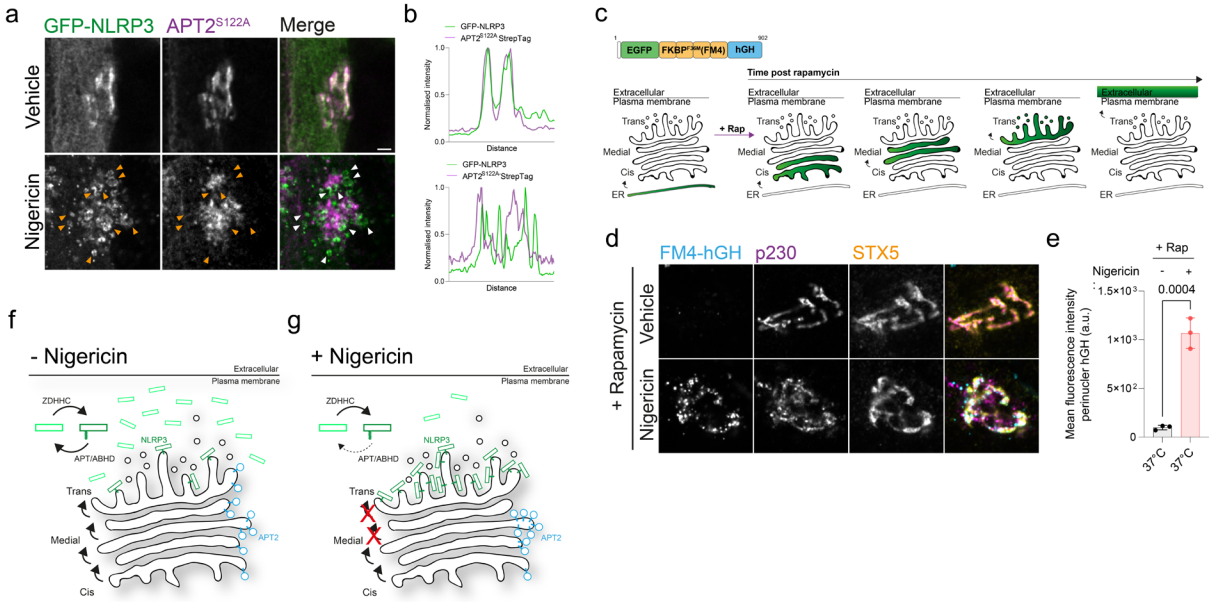

Figure 6. Nigericin inhibits trafficking through the Golgi apparatus and limits contact of thioesterases with NLRP3. A) Representative confocal microscopy images of GFP-NLRP3 and APT2^{S122A}-StrepTag following a 1 hour treatment with 10 µM nigericin or vehicle control. Arrowheads point to instances of GFP-NLRP3 signal where APT2^{S122A} is largely absent. **B)** Linescan analysis of GFP-NLRP3 signal overlap with APT2^{S122A} in control and nigericin treated cells. **C)** Schematic of EGFP-FM4-hGH secretory reporter system showing the domain architecture of the EGFP-FM4-hGH reporter and position of the reporter within the secretory pathway over time after the addition of rapamycin. **D)** Representative confocal microscopy images of EGFP-FM4-hGH relative to the *cis*-Golgi marker STX5 and *trans*-Golgi marker p230 in HeLa cells treated with 500 nM rapamycin, in the presence or absence of 10 µM nigericin, for 1 hour and **E)** quantification of EGFP-FM4-hGH signal in the perinuclear area for the same experiment. N = 3. **F)** Proposed model for S-acylation dependent accumulation of NLRP3 on the Golgi. In the absence of nigericin, NLRP3 shows enrichment on the Golgi due to the balance of acylation and de-acylation provided by the opposing actions of ZDHHC and APT/ABHD enzymes. Access of APT2 to NLRP3 is dependent on anterograde trafficking from cis to trans cisternae remaining intact as APT2 is acylated by ZDHHC3/7, which predominantly localise to the cis-face of the Golgi. **G)** Nigericin inhibits trafficking through the Golgi complex with

476 exchange of material between medial and trans cisternae impaired. This limits the amount of APT2 able to access
477 NLRP3 leading to its gradual accumulation, likely on trans cisternae and the TGN.

478 **Discussion**

479 In this paper we describe the identification of additional features in NLRP3 that are necessary
480 for localisation to the Golgi apparatus. NLRP3 Golgi binding has to date been shown to require
481 interactions between the polybasic region of NLRP3 and PI4P (Chen and Chen, 2018). The
482 NLRP3 polybasic region alone however, is insufficient to achieve localisation of NLRP3 to the
483 Golgi, which is consistent with studies on the mechanistic basis for stable association of
484 peripheral membrane proteins lacking folded lipid binding domains with intracellular
485 membranes (Choy et al., 1999; Hancock et al., 1991; Hancock et al., 1990). Similar to other
486 peripheral membrane proteins that are S-acylated (Chumpen Ramirez et al., 2020; Greaves
487 et al., 2008), electrostatic and hydrophobic interactions with intracellular membranes provided
488 by the polybasic region and helix$^{115-125}$ likely drive an initial low affinity membrane interaction,
489 with stable anchoring to and enrichment on Golgi membranes provided by S-acylation at Cys-
490 130 (**Supplementary Figure 12**). Collectively, Cys-130, helix$^{115-125}$ and the polybasic region
491 form a highly conserved functional unit that are essential for localisation of NLRP3 to the Golgi
492 apparatus and potentially other intracellular membranes.

493 Despite the identification of additional structural features in NLRP3 that are essential for
494 membrane binding, these regions alone are insufficient to achieve Golgi enrichment
495 comparable to full length NLRP3. We could determine a minimal NLRP3 membrane binding
496 region between residues 95-699, which incorporates all the NACHT domain, and part of the
497 trLRR preceding the LRR domain, although this truncated protein failed to accumulate on the
498 Golgi after nigericin treatment to the same degree as the full-length protein. Thus, the LRR
499 appears to play some role in the localisation of NLRP3 to intracellular membranes. Mutations
500 in key residues involved in interactions between the LRR domains of individual NLRP3
501 monomers appear to limit the amount of NLRP3 on the Golgi (Andreeva et al., 2021). LRR
502 dependent formation of an oligomeric NLRP3 complex may therefore increase affinity for
503 intracellular membranes through an avidity-based effect dependent on multiple monomers
504 working together within a larger NLRP3 oligomer. The Cryo-EM structures of NLRP3 are
505 interesting in this respect, as the polybasic regions from multiple monomers appear to be
506 organised within each pentamer / hexamer to form an expanded positively charged docking
507 site around Cys-130 and helix$^{115-125}$ (Andreeva et al., 2021; Hochheiser et al., 2022)
508 (**Supplementary Figure 1A-D**). Membrane contact driven through polybasic / helix$^{115-125}$
509 based multi-valent interactions could then be stabilised by S-acylation at Cys-130 at one or
510 multiple monomers.

511 Consistent with S-acylation controlling NLRP3 localisation, we provide evidence that NLRP3
512 is highly sensitive to levels of ZDHHC3, ZDHHC5, ZDHHC7 and APT2, and that
513 overexpression of ZDHHC3 can sensitise macrophages to nigericin. However we did not
514 identify the endogenous enzymes responsible for stable NLRP3 recruitment to the Golgi
515 through S-acylation and de-acylation, although both ZDHHC3/5/7 and APT2 transcripts are
516 expressed at high levels in THP-1 cells relative to other ZDHHC and APT/ABHD family
517 members (**Supplementary Figure 13**). In agreement with our results showing that localisation
518 of NLRP3 to the Golgi can be controlled by the levels of ZDHHC3/7, a recent pre-print
519 demonstrated that knockout of ZDHHC7 prevents localisation of NLRP3 to the Golgi and limits
520 NLRP3 activation, suggesting that ZDHHC7 is responsible for NLRP3 S-acylation at Cys-130
521 in macrophages (Yu et al., 2023).

522 Our data showing sensitivity of NLRP3 to ZDHHC enzymes localised to distinct organelles
523 (Golgi localised ZDHHC3/7 vs plasma membrane localised ZDHHC5) is intriguing as it
524 suggests NLRP3 can be recruited to different sub-cellular locations through S-acylation at
525 Cys-130, dependent upon PAT abundance and the affinity of NLRP3 for different intracellular
526 membranes dictated by the polybasic region and helix$^{115-126}$. This may help to reconcile our
527 own observations demonstrating NLRP3 association with the Golgi through an S-acylation

528 cycle controlled by Golgi localised palmitoylation machinery, with recent work describing
529 NLRP3 localisation to early and late endosomes in response to NLRP3 agonists, where it is
530 proposed to sense disruptions in endocytic trafficking and ER-endosome contact sites (Lee et
531 al., 2023; Zhang et al., 2023). Alterations in the levels of charged lipids on endosomes caused
532 by NLRP3 stimuli, as has previously been described (Lee et al., 2023; Zhang et al., 2023),
533 could potentially allow NLRP3 to visit endosomal membranes and be trapped there by an
534 endosomally localised PAT. Re-localisation of NLRP3 upon overexpression of ZDHHC5
535 supports the idea that a switch in the use of differentially localised PATs could re-route NLRP3
536 to different sub-cellular compartments including early endosomes, where ZDHHC5 has been
537 proposed to function (Breusegem and Seaman, 2014). An alternative route of endosomal
538 recruitment could also be through a broader inhibition of thioesterase activity, as we observed
539 NLRP3 co-localisation with late endosomes and Rab8^{+} tubular recycling endosomes when de-
540 acylation was inhibited by PalmostatinB, although this re-localisation occurred over the
541 timescale of a number of hours.

542 Membrane binding is required for formation of an inactive oligomeric NLRP3 complex
543 (Andreeva et al., 2021). Disruption of oligomer formation, either through mutation of residues
544 involved in contacts between individual monomers or mutation of the NLRP3 polybasic region,
545 limits NLRP3 activation, suggesting that membrane dependent oligomer formation is essential
546 for sensing of NLRP3 stimuli (Andreeva et al., 2021; Chen and Chen, 2018). Regulation of
547 access to the Golgi through S-acylation at Cys-130 is likely to be important for oligomer
548 formation and may represent another aspect of regulatory control over NLRP3 activation. The
549 steady state balance of S-acylation and de-acylation at Cys-130 may keep levels of Golgi
550 localised NLRP3 below a critical threshold required for further NLRP3 oligomerisation or
551 access to interaction partners and post translational modifications needed for optimal
552 activation. The importance of membrane binding for inflammasome complex formation
553 remains unclear however as two recent studies deleting the region incorporating helix$^{115\text{-}125}$
554 and Cys-130 have produced conflicting results. Deletion of residues 92-120, which removes
555 part of helix$^{115\text{-}125}$, impairs IL1β release, with longer deletions (Δ92-132 and Δ92-148)
556 completely removing Cys-130 and helix$^{115\text{-}125}$ producing an even stronger reduction in
557 inflammasome activation (Tapia-Abellan et al., 2021). In contrast, deletion of exon-3 (spanning
558 residues 95-134), delayed but did not completely block NLRP3 activation as part of a separate
559 study, leading the authors to propose that Golgi binding is not essential for NLRP3 activation
560 (Mateo-Tórtola et al., 2023). In light of the latter study, S-acylation at Cys-130 may accelerate
561 the process of inflammasome formation or increase sensitivity to NLRP3 agonists, although
562 activation can still seemingly occur in the absence of Golgi binding.

563 Based on our mechanism proposing that a nigericin induced block in Golgi trafficking may limit
564 access of thioesterases to NLRP3, enhanced binding of NLRP3 to the Golgi would likely occur
565 in response to any treatment that stops the anterograde flow of membrane from medial to
566 trans cisternae via an effect on Golgi pH or by other means. Enhanced recruitment of NLRP3
567 to the Golgi is therefore not necessarily indicative of NLRP3 activation, given that monensin
568 also triggers accumulation of NLRP3 on the Golgi, although it is worth nothing that monensin
569 can potentiate the effect of weaker NLRP3 agonists (Lee et al., 2023). Whilst the exact reason
570 NLRP3 has evolved to bind to intracellular membranes at present remains unknown, our
571 results nonetheless provide new insight into the mechanisms underpinning membrane
572 recruitment of NLRP3.

573

574 **Methods**

575 **Plasmids**

576 pCMV-APT1-Myc-FLAG and pCMV-APT2-Myc-FLAG were kind gifts from Professor Gisou
577 Van der Goot (École polytechnique fédérale de Lausanne (EPFL), Switzerland). pEGFP-+8-
578 pre was a kind gift from Professor Sergio Grinstein (Hospital for Sick Kids, Ontario, Canada).
579 The HA tagged ZDHHC library containing ZDHHC1-23 was a kind gift from Professor Masaki
580 Fukata (Division of Membrane Physiology, National Institute for Physiological Sciences,
581 Japan). All other plasmids used in this study were cloned using standard molecular biology
582 techniques. In brief, GFP tagged NLRP3 and untagged NLRP3 were amplified and cloned into
583 pIRES Neo between BamHI and NotI sites. For FKBP tagging of GFP tagged WT NLRP3,
584 FKBP was cloned into AgeI and BamHI sites upstream of GFP-NLRP3 in pIRES Neo.
585 $NLRP3^{HF}$, $NLRP3^{PB-1}$ and $NLRP3^{PB-2}$ were made by extension overlap PCR from wild type
586 GFP tagged NLRP3 and cloned into pIRES Neo between BamHI and NotI sites. For point
587 mutations in NLRP3 and ZDHHC3, an NEB Q5 SDM kit (NEB, E0554S) was used, followed
588 by sequencing of clones to confirm the presence of the correct mutation. For generation of
589 APT2-StrepTag-FKBP, StrepTag-FKBP was cloned between PmeI and NotI sites in at the C-
590 terminus of APT2 in pCMV. For generation of the minimal NLRP3 constructs spanning
591 residues 95-158 and variants thereof, GFP was first cloned into pIRES neo between AgeI and
592 BamHI sites before insertion of the $NLRP3^{95-158}$ sequences between BamHI and NotI sites.
593 For pLXIN constructs, all inserts were cloned between BamHI and NotI sites in pLXIN. Primer
594 details for all constructs described are available upon request.

595 **Antibodies**

596 Anti-TGN46 (Bio-rad, APH500GT), anti-HA (Biolegend, 901502), anti-NLRP3 (Abcam,
597 Ab4207), anti-NLRP3 (adipogen, AG-20B-0014-C100), anti-Rab8 (Cell signalling, Cat-no
598 6975), anti-CD63 (H5C6), anti-p230 (BD-biosciences, 611280), anti-tubulin (Protein-tech,
599 66240-1-1g), anti-STX5 (Synaptic systems, 110053). Secondary antibodies used for western
600 blotting were HRP conjugated goat anti-mouse (1:2000, Jackson Immuno Research 115-035-
601 008) and HRP conjugated goat anti-rabbit (1:2000, Jackson Immuno Research 111-035-144).
602 Secondary antibodies used for immunofluorescence were donkey anti-rabbit Alexa-488
603 (ThermoFisher, A-21206), donkey anti-rabbit Alexa-594 (ThermoFisher, A-21207), donkey
604 anti-rabbit Alexa-647 (ThermoFisher, A-31573), donkey anti-mouse Alexa-488 (ThermoFisher,
605 A-21202), donkey anti-mouse Alexa-594 (ThermoFisher, A-21203), donkey anti-mouse Alexa-
606 647(ThermoFisher, A-31571), chicken anti-rabbit Alexa-647 (ThermoFisher, A-21443),
607 chicken anti-mouse Alexa-647 (ThermoFisher, A-21463), donkey anti-goat 594
608 (ThermoFisher, A-11058).

609 **Cell culture**

610 HeLaM cells were originally obtained from the laboratory of Margaret S. Robinson (Cambridge
611 Institute of Medical Research, University of Cambridge, UK). HEK-293T cells were obtained
612 from ATCC. THP-1 cells were a kind gift from Professor Paul Lehner, University of Cambridge.
613 HeLa cells stably expressing EGFP-FM4-hGH were generated in house and described
614 previously (Gordon et al., 2010; Gordon et al., 2021). HeLa, HeLaM and HEK-293T cells were
615 grown in Dulbeccos modified Eagles medium (DMEM) (Merck, D6429-500ML) supplemented
616 with 10% Foetal bovine serum (FBS) (Merck, F4135-500ML), 100 IU/ml pencillin and 100 µg
617 / ml streptomycin (Merck, G1146-100ML) at 37°C in a 5% CO_2 humidified incubator. THP-1
618 cells were grown in Roswell Park Memorial Institute (RPMI) 1640 medium (Merck, R8758-
619 500ML) supplemented with 10% FBS, 100 IU / ml pencillin, 100 µg / ml streptomycin and 2
620 mM L-glutamine (Fisher Scientific Ltd, 10691233) at 37 °C in a 5% CO_2 humidified incubator.

621 **Generation of stable cell lines**

622 For generation of all stable THP-1 cell lines, a second-generation retroviral vector system was
623 used. Briefly, HEK-293T cells seeded into 12 well plates were transfected with the retroviral

packaging plasmid pUMVC (Addgene: 8449), pLXIN (Clontech, 631501) containing the gene of interest and pCMV VSV-G at a ratio of 5:5:1 with polyethylenimine (PEI) (1 µg DNA to 3 µg PEI). 48 hours post transfection, cell culture media was harvested and clarified by centrifugation to pellet loose cells. The supernatant was collected and, after addition of polybrene to a final concentration of 10 µg / ml, viral media was then added to THP-1 cells. The THP-1 cell-viral media suspension was then centrifuged at 2500 x g for 90 minutes at room temperature. Cells were incubated at 37°C and successfully transduced cells selected by addition of 1 mg / ml G418 (SLS, 4727878001) to the cell media for 1 week.

Transfections and Immunofluorescence

HeLaM cells were seeded onto glass coverslips in 12 well plates at a density of 2.25 x 10^5 cells / well and left to adhere overnight. The next day cells were transfected with plasmid DNA using Viafect (E4982, Promega) at a ratio of 3:1 viafect to DNA, according to the manufacturer's instructions. Cells were then incubated overnight at 37°C and processed the next day. For HeLaM and THP-1 cell staining's, cells were pre-fixed by addition of an equivalent volume of 4% paraformaldehyde (PFA, Park Scientific Limited, 04018-4) to cell culture media for 1 minute. PFA-media solution was aspirated, and cells were then incubated with 4% PFA for 10 minutes at room temperature. After aspirating, cells were incubated with 100mM Glycine (Merck, G7126) in PBS for 3 minutes to quench PFA. Glycine was then aspirated and cells permeabilised and blocked for 5 minutes with PBS containing 1% bovine serum albumin (BSA) (BP1600-100, Fisher Scientific) and 0.1% saponin (84510-100G, Merck) (IF buffer). Cells were incubated with primary antibody solutions in IF buffer for 30 minutes at 37°C before being washed three times with IF buffer. Cells were then incubated with secondary antibodies in IF buffer for a further 30 minutes at 37°C. Following secondary antibody incubation cells were washed a further 3 times with IF buffer before a final wash in PBS. Coverslips were mounted onto glass slides using prolong gold antifade (ThermoFisher Scientific, P36930). Coverslips were imaged on a Nikon A1 upright confocal microscope with a 60x, NA 1.4, Plan Apochromat oil immersion objective with approximately 1.4x digital zoom added at a pixel resolution of 1024 x 1024.

Fluorescence recovery after photobleaching (FRAP)

Cells were seeded overnight at a density of 2.25 x 10^5 / quarter of a cellview cell culture dish (Greiner Bio, 627870) and transfected with GFP-NLRP3 the next day. FRAP experiments were performed on a Zeiss LSM880 airyscan confocal microscope using a 63X 1.4 NA Plan Apochromat oil immersion objective with a temperature-controlled stage set to 37°C. For FRAP experiments, the entire Golgi region was photobleached using the 405nm laser-line before images were acquired at 3 second intervals for a period of 6 minutes. Recovery curves were generated by measurement of GFP intensity in the bleached area at each individual timepoint and were adjusted for fluorescence decay caused by prolonged imaging during the recovery period. The immobile and mobile pools of NLRP3 were calculated by the following formula:

Mobile fraction = $(MFI^{final} – MFI^{bleach}) / (MFI^{pre\text{-}bleach} – MFI^{bleach})$

Immboile fraction = $1 - (MFI^{final} – MFI^{bleach}) / (MFI^{pre\text{-}bleach} – MFI^{bleach})$

Where MFI^{final} corresponds to the mean fluorescence intensity (MFI) in the bleach area at the final recovery timepoint post-bleach, MFI^{bleach} corresponds to the MFI in the bleach area immediately after photobleaching and $MFI^{pre\text{-}bleach}$ corresponds to the MFI in the bleach area prior to photobleaching. Recovery half times were calculated using EasyFRAP software (Koulouras et al., 2018).

Inflammasome assays

THP1 cells were seeded into 96 well plates in RPMI containing 100 ng / µl PMA (PMA) (Merck, P1585) and left to adhere overnight at 37 °C. The next day, PMA was aspirated and cells

673 incubated with RPMI containing 1 µg / ml LPS (Merck, L2630) for 3 hours. Prior to nigericin
674 stimulation, cells were washed once with PBS and incubated with a solution containing LPS
675 and 1 µg / ml wheat germ agglutinin-Alexa-647 (WGA) (Thermo Fisher Scientific, W3246,) for
676 10 minutes to visualise the plasma membrane and facilitate quantification. Cells were washed
677 once with PBS and then incubated with RPMI containing 1 µg / ml propidium iodide (PI) (Merck)
678 and nigericin (Merck, N7143) (20 µg / ml) for two hours before imaging live on a Nikon A1
679 upright confocal microscope. Per experiment, a minimum of 4 separate fields of view per cell
680 line were acquired and the number of live cells and dead cells counted manually based on the
681 presence of propidium iodide.

682 **PEG switch assay**

683 HeLaM cells were seeded into 12 well plates and transfected as described above. The next
684 day cells were lysed in 200 µl of PEG switch sample buffer (PS buffer) (1% SDS, 50 mM
685 HEPES) supplemented with 100 mM NEM (Merck, E3876), 1 mM PMSF (Merck, P7626-1G)
686 and 1X protease inhibitor cocktail (Merck, 11873580001) for 30 minutes at room temperature.
687 Cell lysates were incubated at 40°C with shaking for 4 hours to block free cysteine residues.
688 Following this, to remove NEM and precipitate proteins, 4 volumes of 100% acetone were
689 added to lysates and incubated for 1 hour at -20°C before lysates were centrifuged at 15,000
690 x g for 10 minutes to pellet precipitated proteins. The acetone-sample buffer mix was aspirated,
691 and protein pellets were washed 4 times with 70% acetone to remove residual NEM. After the
692 final wash, acetone was aspirated and protein pellets dried at room temperature for 10 minutes.
693 Pellets were resuspended in 200 µl PS buffer before the sample was split in two and either
694 0.4M hydroxylamine (SLS, 159417-100G) or water added. Samples were incubated for 1 hour
695 at 37°C before proteins were again acetone precipitated for 1 hour as described above. Pellets
696 were washed once more with 70% acetone, air-dried for 10 minutes and resuspended in 100
697 µl PS buffer. 2 mM PEG-maleimide was then added to label exposed S-acylated cysteine
698 residues and samples incubated for 1 hour at 37°C. Following addition of SDS-PAGE sample
699 buffer the samples were boiled for 5 minutes at 95 °C and resolved by SDS-PAGE.

700 **Western blotting**

701 SDS-PAGE sample buffer (BioRad, 1610747) supplemented with 5% (v/v) mercaptoethanol
702 was added to samples lysed in PS buffer before boiling for 5 minutes at 95°C. Samples were
703 then loaded onto an appropriate percentage Tris-Glycine polyacrylamide gel and proteins
704 resolved by SDS-PAGE. Gels were transferred to PVDF membrane using a BioRad semi-dry
705 transfer system. Following transfer, membranes were blocked in 5% milk in PBS containing
706 0.1% Triton X-100 (PBSTx) for a minimum of 30 minutes. Blocked membranes were incubated
707 with primary antibodies diluted in PBSTx and 5% milk overnight at 4°C. The next day, unbound
708 antibodies were removed by 3 x 5 minute washes in PBSTx before incubation with secondary
709 antibodies in PBSTx containing 5% milk for 1 hour with rotation at room temperature.
710 Membranes were again washed 3 times for 5 minutes with PBSTx and signal detected using
711 BioRad ECL chemiluminescence substrate and the LiCor c-digit system.

712 **Quantification and statistical analysis**

713 For quantification of Golgi associated NLRP3 signal in untreated and nigericin treated cells,
714 the Golgi region was identified using a Golgi marker which remains associated with the Golgi
715 following nigericin treatment (either GM130 or p230) and the amount of NLRP3 associated
716 measured through manual segmentation of the Golgi region in FIJI (Schindelin et al., 2012).
717 An equivalent area of GFP-NLRP3 signal in the cytosol away from the perinuclear region was
718 measured and the ratio between the Golgi NLRP3 signal and cytosolic NLRP3 signal
719 calculated for each cell expressing GFP-NLRP3. All N numbers represent a minimum of 20
720 cells quantified per experiment with each graphed datapoint representing an independent
721 experiment performed on separate days. All graphs included in figures were made using the
722 GraphPad Prism software package. Statistical comparisons between groups using an
723 unpaired t-test were all performed using GraphPad Prism 9.0.

Acknowledgements

We are grateful to the University of Sheffield Wolfson Light microscopy facility for technical support with microscopy experiments. We also thank Dr Mark Collins (University of Sheffield), for advice on acylation assays and Professor Martin Lowe (University of Manchester) and Dr Xiaoming Fang (University of Cambridge) for helpful discussions and advice on the manuscript. A.P. and D.W. are supported by the BBSRC (BB/S009566/1).

731 **Supplementary Figures**

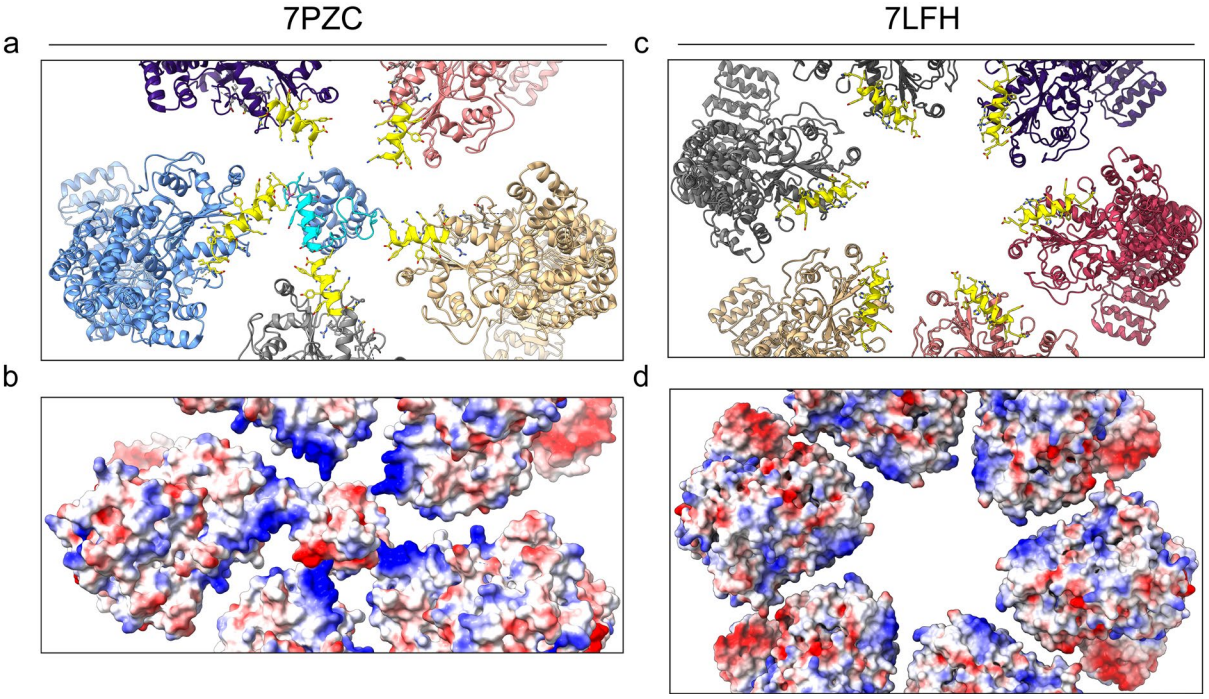

732

733

734 **Supplementary Figure 1. Cysteine-130 is surface exposed in the cryo-EM structure of the inactive NLRP3**
735 **complex. A)** View of an individual NLRP3 pentamer from 7PZC and **C)** an NLRP3 hexamer from 7LFH looking
736 into the core of the decameric complex, where the PYD domains are proposed to be shielded. For 7PZC, the
737 polybasic regions from each monomer are arranged around helix$^{115\text{-}125}$ and Cys-130, with a similar arrangement
738 seen in 7FLH, although helix$^{115\text{-}125}$ and Cys-130 were not resolved in 7FLH. Electrostatic potential of the polybasic
739 regions from each monomer surrounding helix$^{115\text{-}125}$ and Cys-130 mapped onto the structure of the NLRP3
740 pentamer for **B)** 7PZC and the NLRP3 hexamer for **D)** 7LFH.

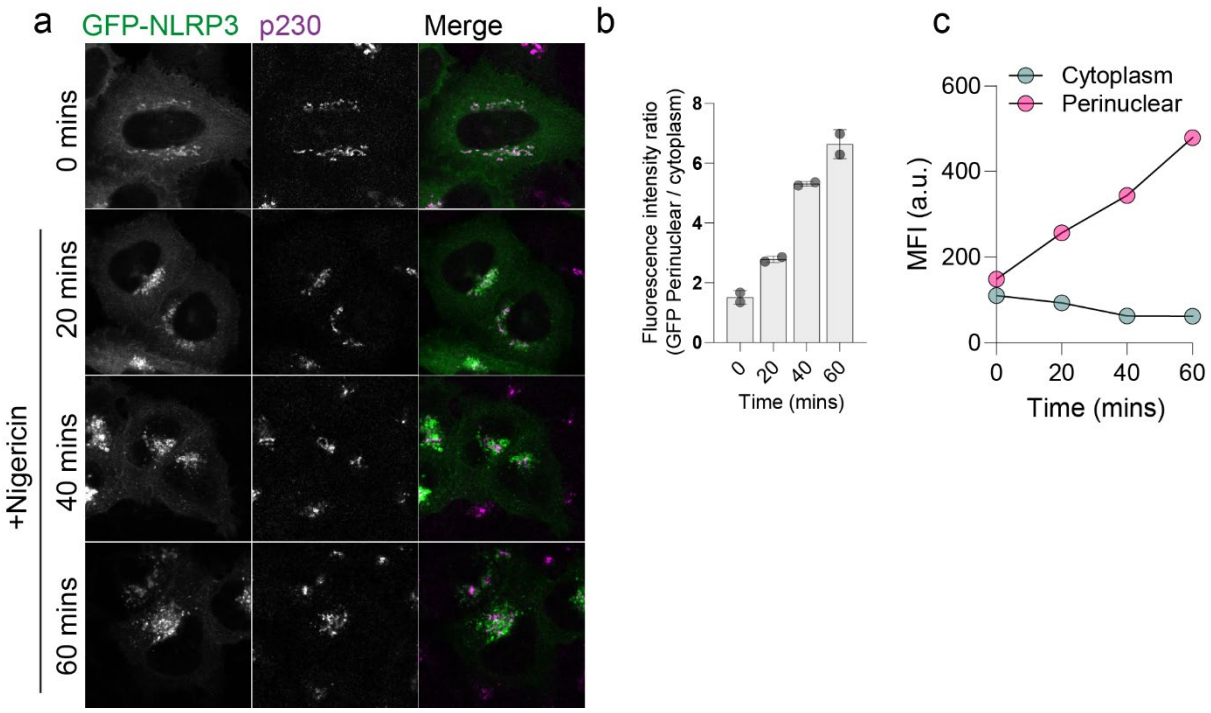

741

742

743 **Supplementary Figure 2. Dynamics of NLRP3 association with the Golgi post nigericin treatment in HeLaM**
744 **cells. A)** Representative images of GFP-NLRP3 transiently expressed in HeLaM cells treated with 10 μM nigericin
745 for the indicated times. Scale bar = 10 μm **B)** Quantification of the Golgi to cytoplasmic GFP-NLRP3 fluorescence
746 for the same experiment. N = 2. **C)** Mean fluorescence intensity values (MFI) for GFP-NLRP3 in the cytosol and
747 Golgi from cells treated with 10μM nigericin for the indicated times.

748

749

750

751

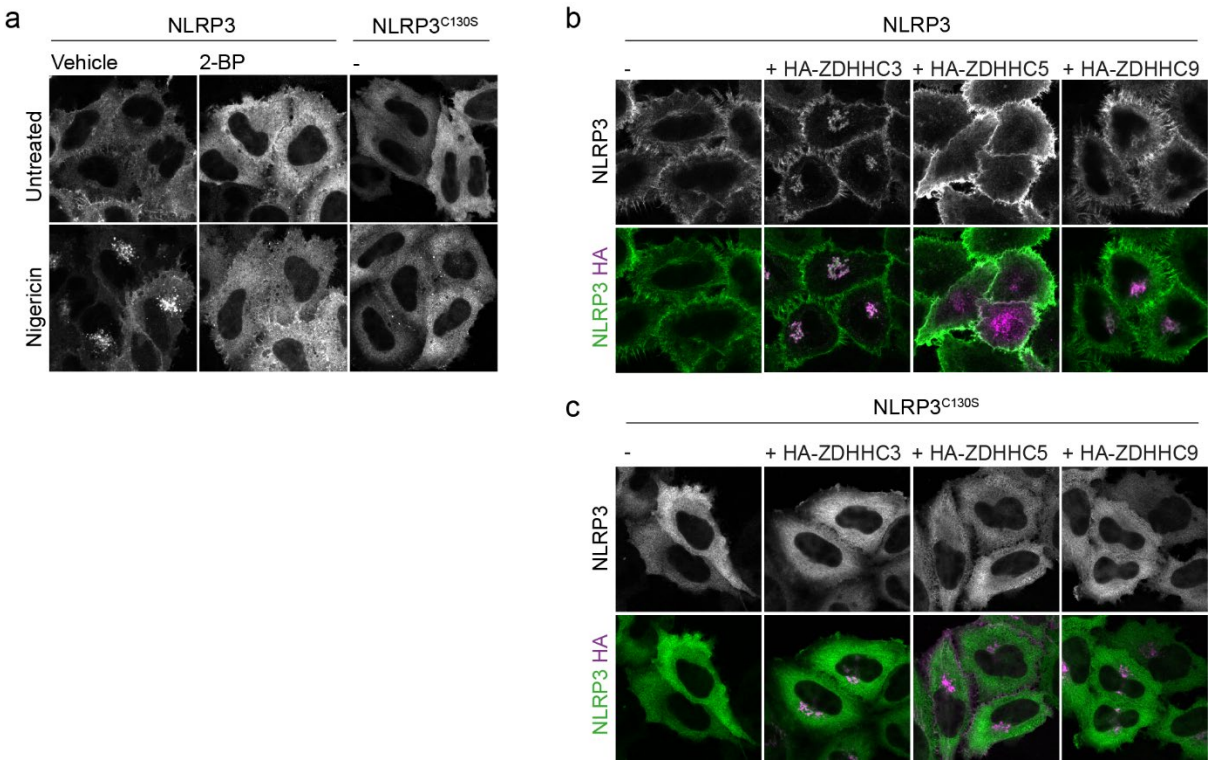

Supplementary Figure 3. Localisation of untagged NLRP3 to the Golgi is S-acylation dependent. A) Representative confocal microscopy images of HeLaM cells transiently expressing untagged NLRP3 or NLRP3^{C130S} visualised with anti-NLRP3 antibodies. Cells were treated with either 0.5% DMSO or 100 µM 2-BP for 16 hours before treatment with 10 µM nigericin or vehicle for 1 hour. Representative confocal microscopy images of HeLaM cells transiently transfected with **B)** NLRP3 or **C)** NLRP3^{C130S} and 0.25 µg of the indicated ZDHHC enzyme. Untagged NLRP3 is sensitive to the same ZDHHC enzymes in a Cys-130 dependent manner as GFP tagged NLRP3.

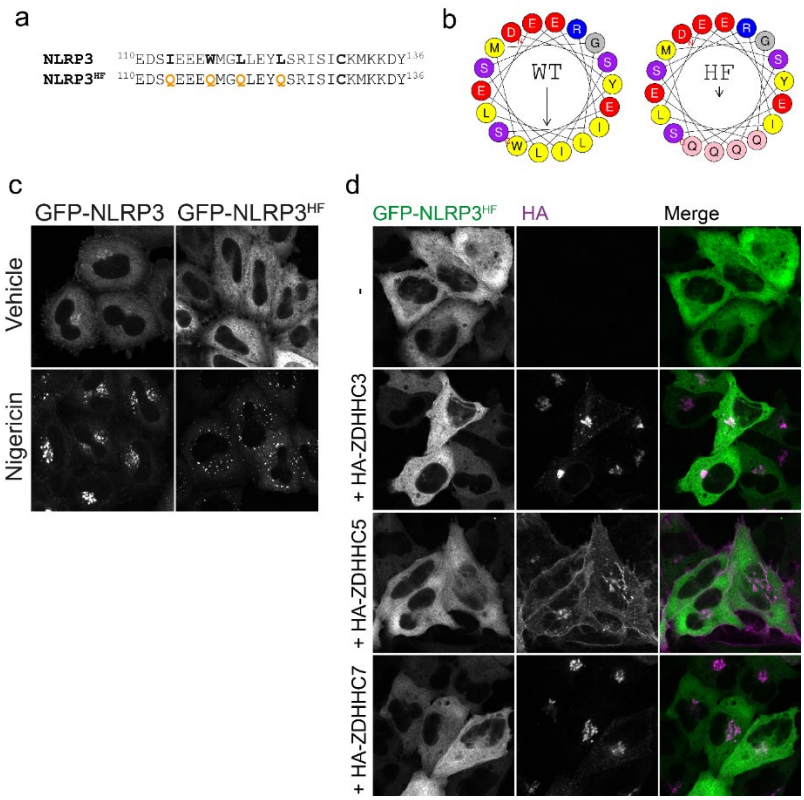

Supplementary Figure 4. Hydrophobic residues within helix$^{115\text{-}125}$ are important for localisation of NLRP3 to the Golgi apparatus. A) Sequence of NLRP3 between residues 110 and 136 and mutations made in the same sequence to disrupt the putative hydrophobic face of helix$^{115\text{-}125}$. **B)** Heliquest plot of wild type NLRP3 sequence for residues 111-128 and the effect of mutations to residues I113, W117, L120 and L124 (NLRP3^{HF}) on the hydrophobic face. **C)** Representative images of wild type GFP-NLRP3 and GFP-NLRP3^{HF} transiently expressed in HeLaM cells and treated with 10 µM nigericin for 1hour or left untreated. **D)** GFP-NLRP3^{HF} is insensitive to ZDHHC overexpression. Representative images of HeLaM cells transfected with GFP-NLRP3^{HF} and 0.25 µg of the indicated HA-ZDHHC enzyme.

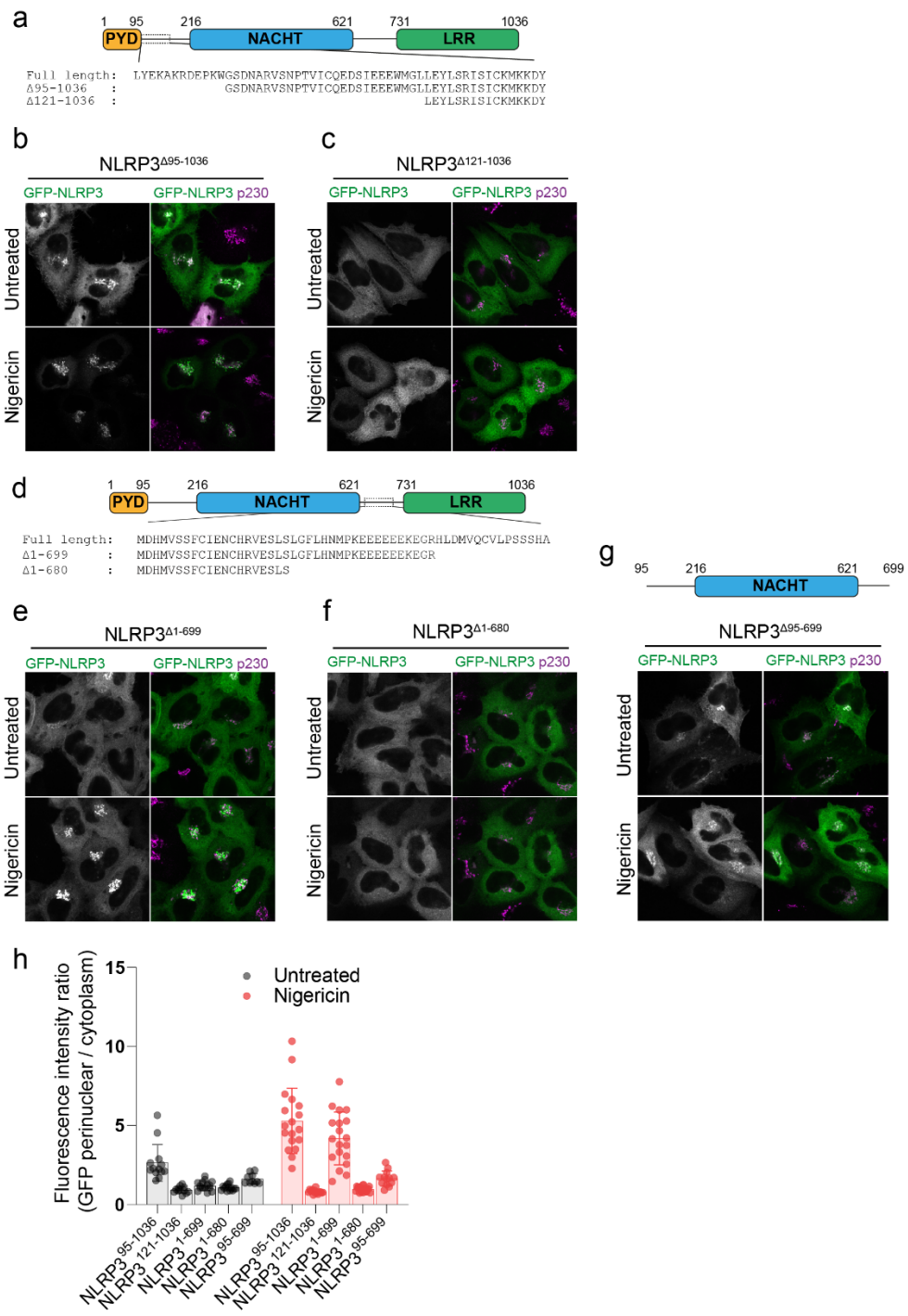

Supplementary Figure 5. Definition of a minimal NLRP3 region required for enrichment at the Golgi apparatus. A) Schematic of truncations made in full length NLRP3 from the N terminus of the protein. Representative confocal microscopy images of **B)** GFP-NLRP3$^{\Delta 95\text{-}1036}$ or **C)** GFP-NLRP3$^{\Delta 121\text{-}1036}$ transiently expressed in HeLaM cells, treated with or without 10 μM nigericin for 1 hour. **D)** Schematic of truncations made in full length NLRP3 from the C terminus of the protein. Representative confocal microscopy images of the **E)** GFP-NLRP3$^{\Delta 1\text{-}699}$ or **F)** GFP-NLRP3$^{\Delta 1\text{-}680}$ transiently expressed in HeLaM cells, treated with or without 10 μM nigericin for 1 hour. **G)** Schematic of the minimal Golgi binding truncation mutant NLRP3 $^{\Delta 95\text{-}699}$ with representative confocal microscopy images of NLRP3 $^{\Delta 95\text{-}699}$ expressed in HeLaM cells, treated with or without 10 μM nigericin for 1 hour. **H)** Quantification of the ratio of GFP signal in the perinuclear region over cytoplasmic GFP signal for each of the indicated constructs.

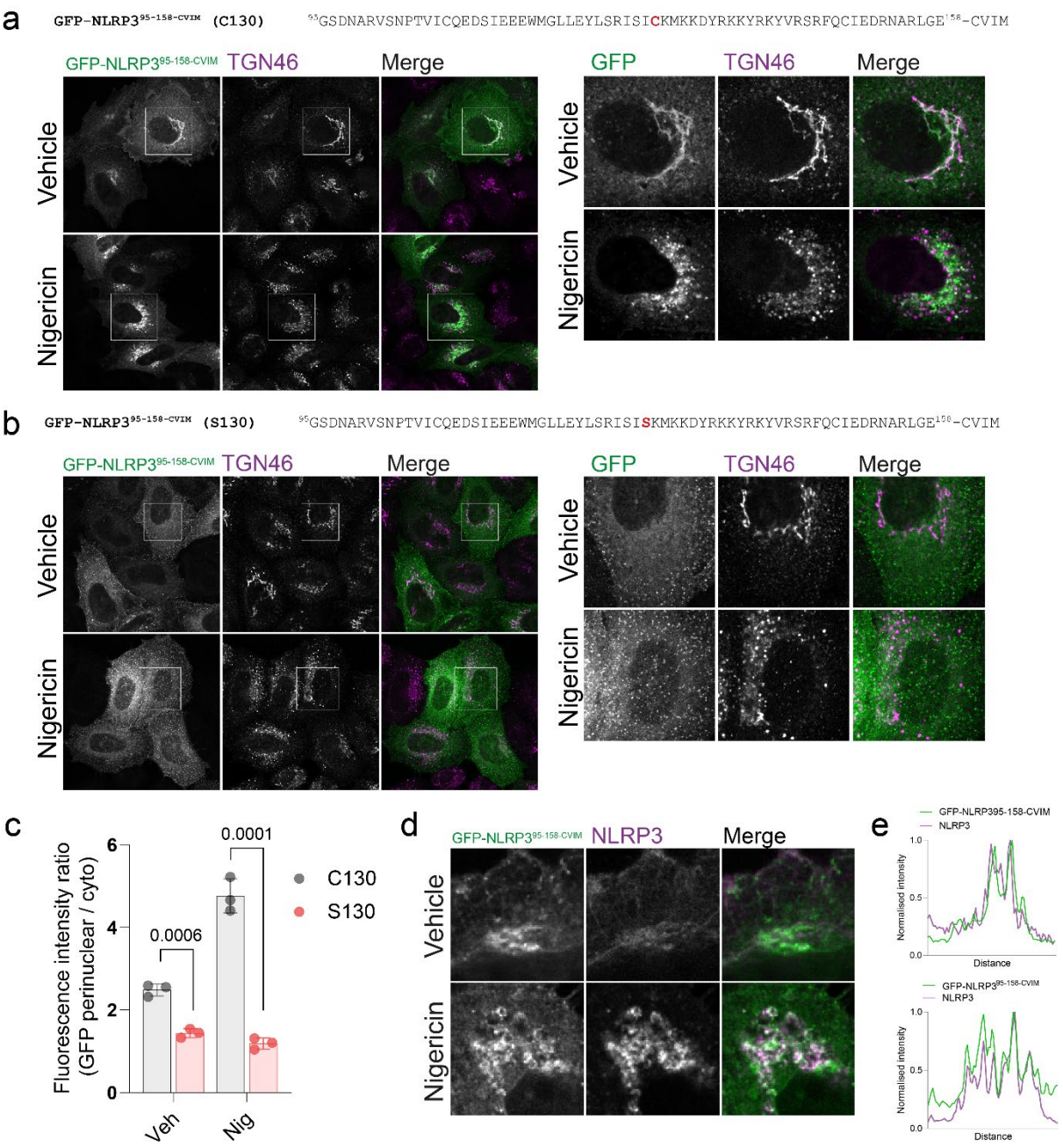

Supplementary Figure 6. Farnesylation of NLRP3 residues 95-158 permits Cys-130 dependent Golgi association. A) Representative images of NLRP3$^{95\text{-}158\text{-}CVIM}$ and **B)** NLRP3$^{C130S,95\text{-}158\text{-}CVIM}$ transiently expressed in HeLaM cells treated with or without 10 μM nigericin for 1 hour. Boxed region in each image indicates the region shown in higher magnification next to each set of images. **C)** Quantification of the Golgi association of each construct in untreated cells and in cells treated with 10 μM Nigericin for 1 hour. **D)** Representative microscopy images showing GFP-NLRP3$^{95\text{-}158\text{-}CVIM}$ co-localisation with untagged NLRP3 in untreated cells and following nigericin stimulation. Cells were stimulated with 10 μM nigericin or vehicle for 1 hour. **E)** Linescan analysis of GFP-NLRP3$^{95\text{-}158\text{-}CVIM}$ signal with NLRP3 in vehicle treated and nigericin treated cells. GFP-NLRP3$^{95\text{-}158\text{-}CVIM}$ shows a high degree of overlap with NLRP3 under both conditions.

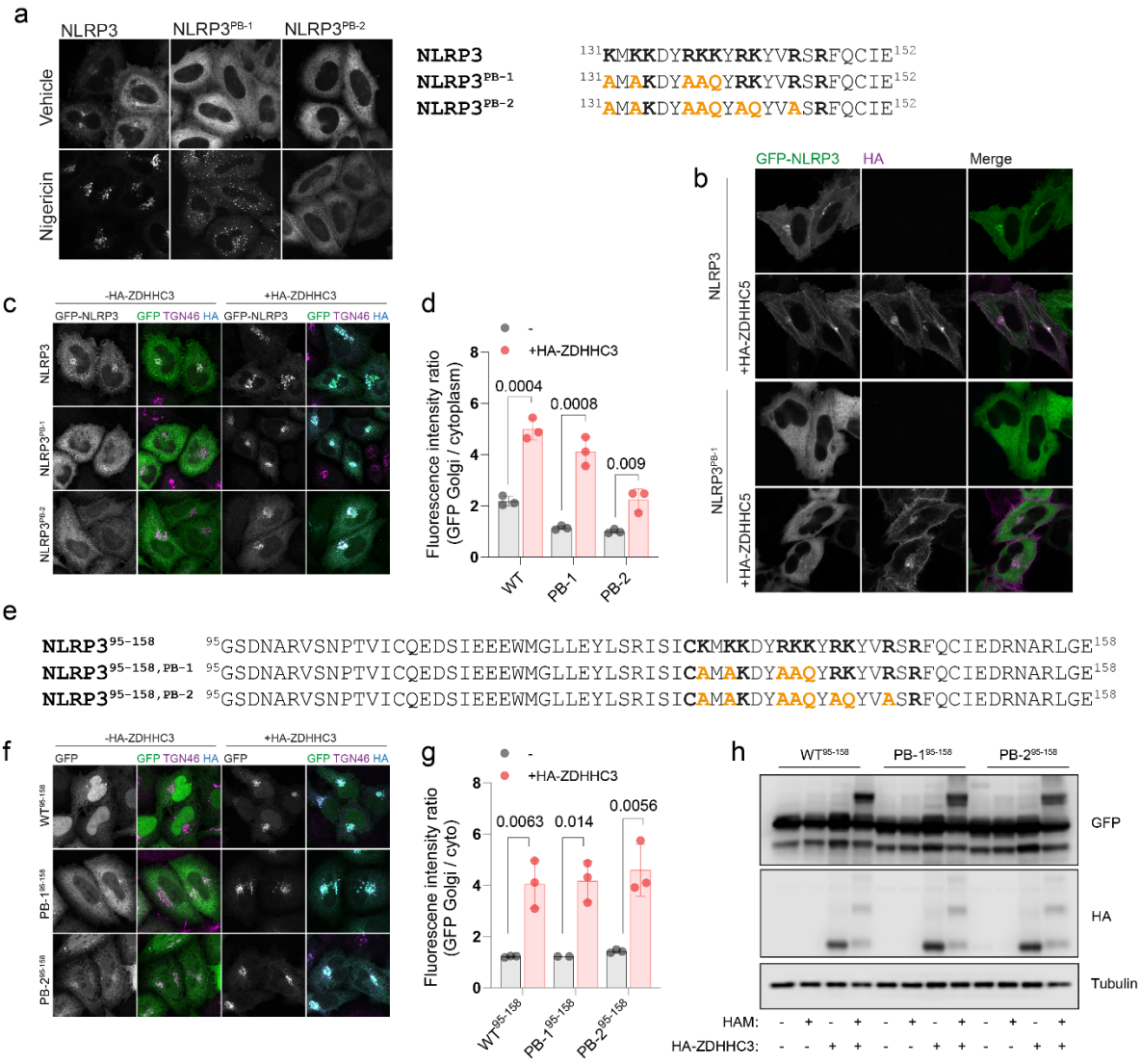

Supplementary Figure 7. Requirement of the NLRP3 polybasic region for sensitivity to ZDHHC3 and ZDHHC5. A) Reperesentative images of full length GFP tagged NLRP3 polybasic mutants treated with or without 10 µM nigericin for 1 hour and schematic of mutations made in the polybasic region. Mutated residues are highlighted in orange. **B)** Representative images of GFP-NLRP3 and GFP-NLRP3^{PB-1} coexpressed with or without HA-ZDHHC5. Mutation of residues within the polybasic region renders NLRP3 insensitive to ZDHHC5 overexpression. **C)** Representative confocal microscopy images of GFP-NLRP3, GFP-NLRP3^{PB-1} and GFP-NLRP3^{PB-2} transiently expressed in HeLaM cells alone or with HA-ZDHHC3. **D)** Quantification of GFP-NLRP3, GFP-NLRP3^{PB-1} and GFP-NLRP3^{PB-2} Golgi recruitment with and without HA-ZDHHC3. **E)** Schematic of mutations made in the polybasic region of GFP-NLRP3$^{95-158}$ constructs. Mutated residues are highlighted in orange. **F)** Representative confocal microscopy images of GFP-NLRP3$^{95-158}$, GFP-NLRP3$^{PB-1,95-158}$ or GFP-NLRP3$^{PB-2,95-158}$ expressed in HeLaM cells with or without HA-ZDHHC3. **G)** Quantification of GFP-NLRP3$^{95-158}$, GFP-NLRP3$^{PB-1,95-158}$ or GFP-NLRP3$^{PB-2,95-158}$ signal on the Golgi with and without HA-ZDHHC3. **H)** Western blots of acyl biotin exchange assay using 5kDa PEG maleimide performed on cell lysates harvested from cells expressing GFP-NLRP3$^{95-158}$, GFP-NLRP3 $^{PB-1,95-158}$ or GFP-NLRP3$^{PB-2,95-158}$ with or without HA-ZDHHC3.

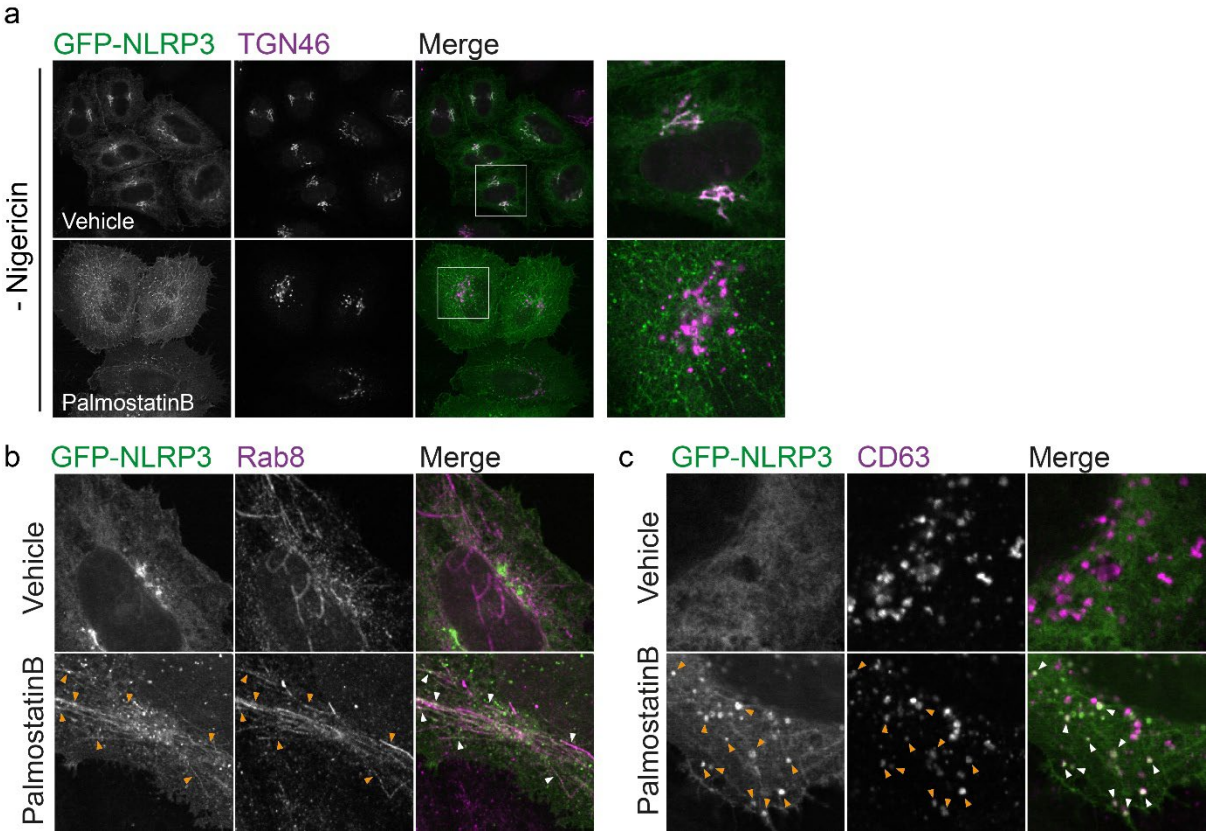

Supplementary Figure 8. PalmostatinB treatment relocalises NLRP3 to the plasma membrane, tubular recycling endosomes and late endosomes. A) Zoom out of images from Figure 5A showing multiple cells treated with vehicle or 50 μM Palmostatin B for 4 hours. Representative images of GFP-NLRP3 co-localisation with **B)** Rab8 or **C)** CD63 in cells treated with vehicle or 50 μM PalmostatinB for 4 hours. Orange arrowheads point to instances of co-localisation between GFP-NLRP3 and the indicated marker in PalmostatinB treated cells.

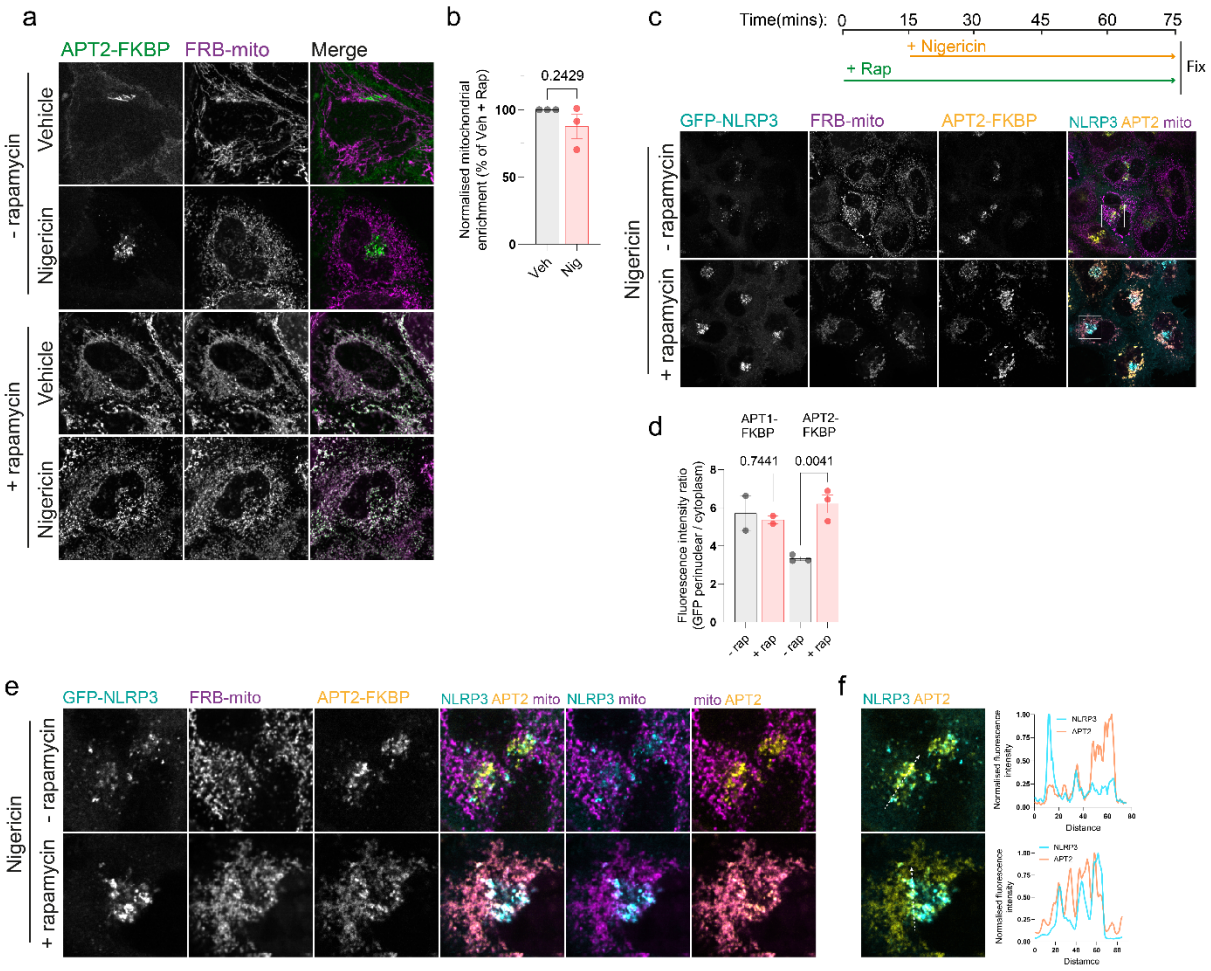

Supplementary Figure 9. The effect of APT2 on NLRP3 Golgi enrichment can be reversed. A) Representative confocal microscopy images and quantification of APT2-StrepTag-FKBP (APT2) signal in the perinuclear region showing re-routing of APT2 onto mitochondrial membranes in the presence of 500 nM rapamycin for 15 minutes and **B)** Quantification of APT2 signal recruited to the mitochondria relative to cytosolic signal with and without 10 µM nigericin. Nigericin treatment has no significant effect on recruitment of APT2 to the mitochondria. **C)** Representative images of HeLaM cells transiently expressing GFP-NLRP3 with APT2-StrepTag-FKBP and FRB-mito pre-treated with rapamycin or vehicle for 15 minutes prior to 10 µM nigericin treatment for 1 hour. Removal of overexpressed APT2-StrepTag-FKBP activity restores the enhanced perinuclear NLRP3 signal seen following nigericin treatment to levels seen using APT1, quantified in **D)**. **E)** Zoom in of boxed regions in C) showing overlap between GFP-NLRP3 and APT2-StrepTag with **F)** linescan analysis for each set of images.

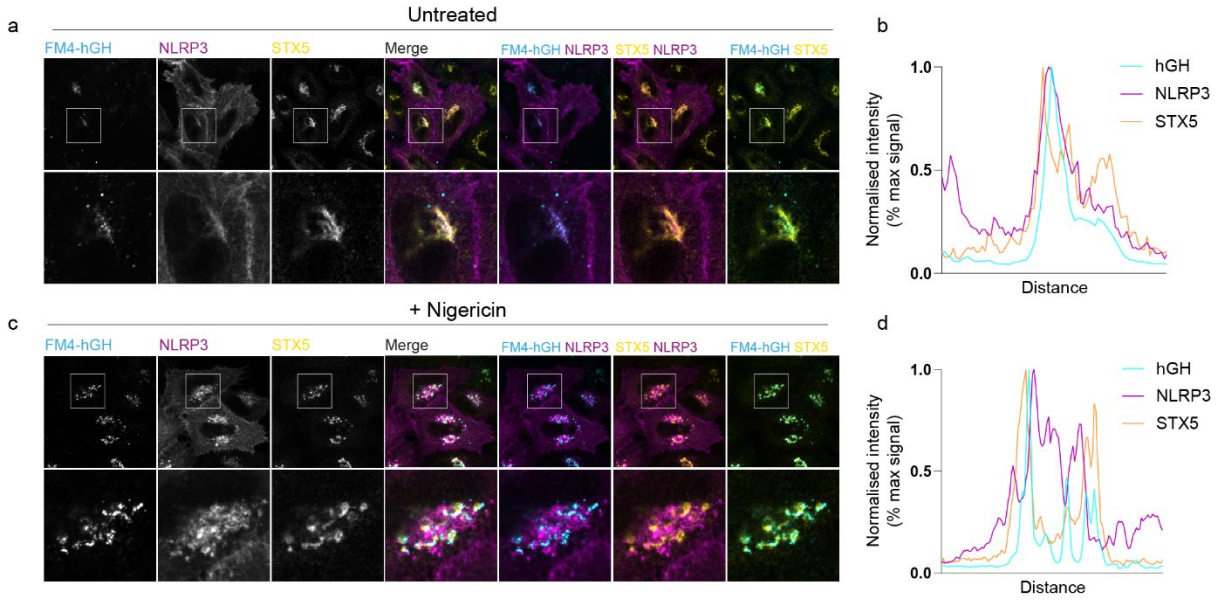

Supplementary Figure 10. NLRP3 accumulates on Golgi compartments that are distinct from the cis-Golgi after nigericin treatment. Representative images of untagged NLRP3 expressed in HeLa cells stably expressing the secretory reporter EGFP-FM4-hGH, treated with 500nM rapamycin for 1 hour in the **A)** absence or **C)** presence of nigericin. Following nigericin treatment, NLRP3 shows minimal co-localisation with the cis Golgi marker STX5 and hGH, which is trapped in STX5^{+} compartments. Line scan analysis of NLRP3 signal overlap with hGH and STX5 in **B)** vehicle treated control cells or **D)** cells treated with 10 μM nigericin for 1 hour.

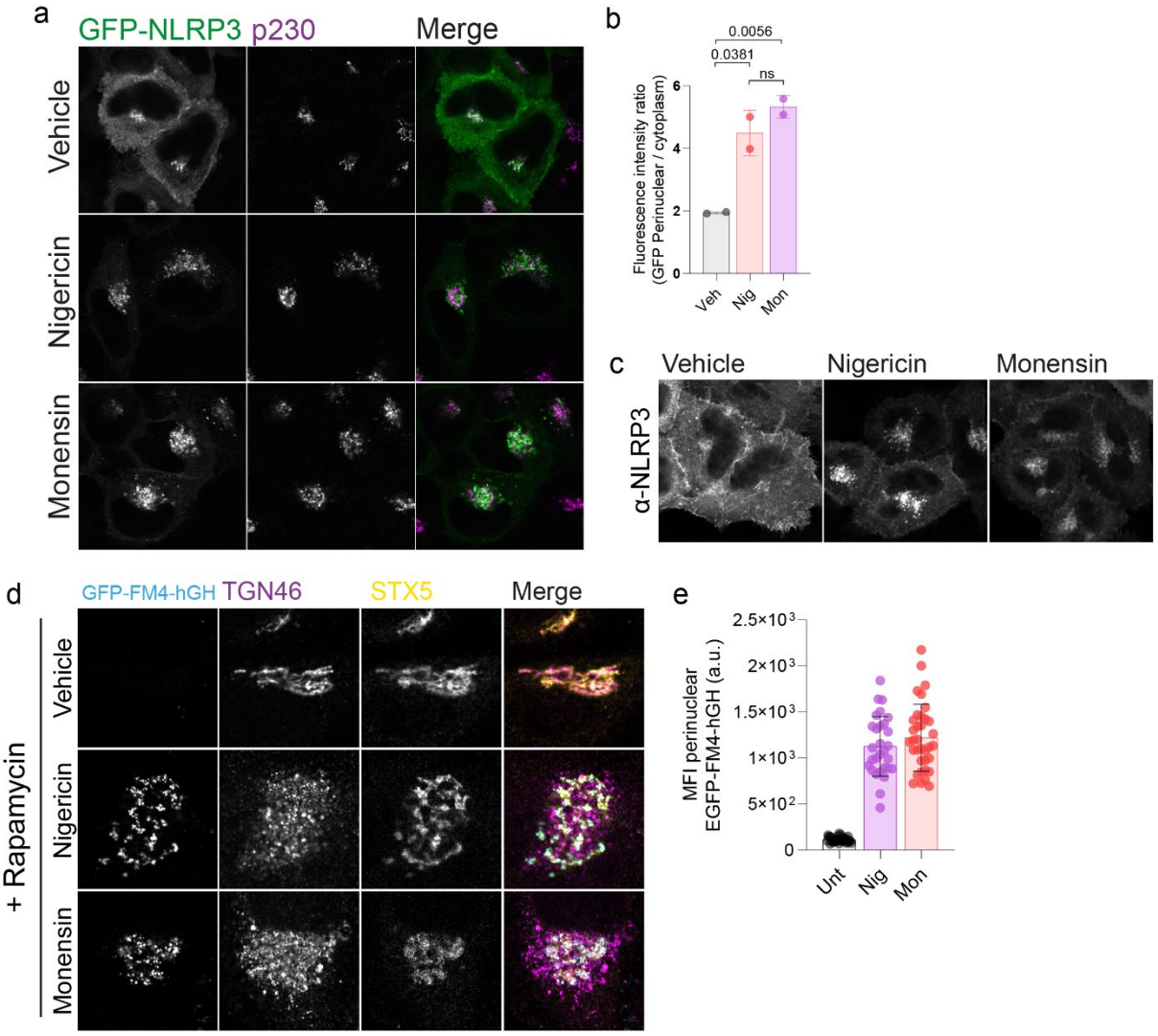

Supplementary figure 11. Monensin enhances NLRP3 Golgi recruitment and blocks trafficking through the Golgi. A) Representative images of HeLaM cells transfected with GFP-NLRP3 and treated with either 10 μM nigericin or 10 μM monensin for 1 hour. Scale bar = 10 μm. **B)** Quantification of the Golgi to cytoplasmic GFP-NLRP3 ratio following treatment with nigericin or monensin. N=2. **C)** Representative images of HeLaM cells transfected with an untagged NLRP3 construct and stained with anti-NLRP3 antibodies following treatment with either 10 μM nigericin or 10 μM monensin for 1 hour. Scale bar = 10 μm. **D)** Representative images of HeLa EGFP-FM4-hGH cells treated with 10 μM nigericin or 10 μM monensin for 1 hour in the presence of rapamycin to solubilise aggregated cargo in the ER. **E)** Quantification of EGFP-FM4-hGH signal in the perinuclear region.

a

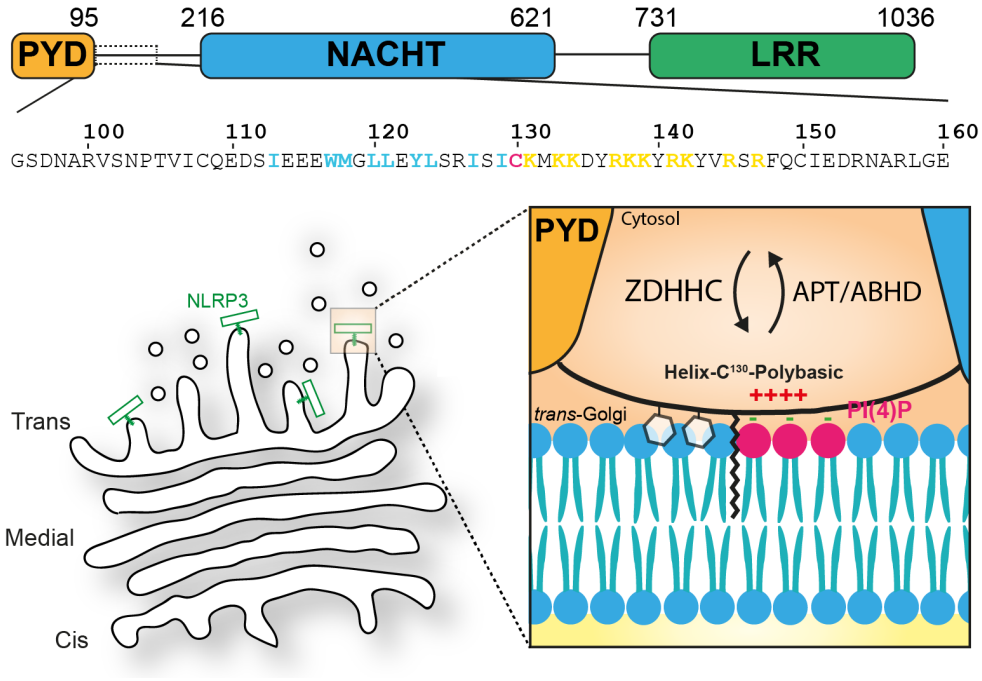

Supplementary figure 12. Model of S-acylation dependent recruitment of NLRP3 to intracellular membranes. A) Interaction of NLRP3 with intracellular membranes is likely to be driven through a initial transient mode of binding provided by residues in helix$^{115\text{-}125}$ and the polybasic region. Stable enrichment and trapping of NLRP3 at the Golgi requires S-acylation at Cys-130 by ZDHHC enzymes with removal of NLRP3 likely catalysed by proteins from the APT or ABHD family of thioesterases.

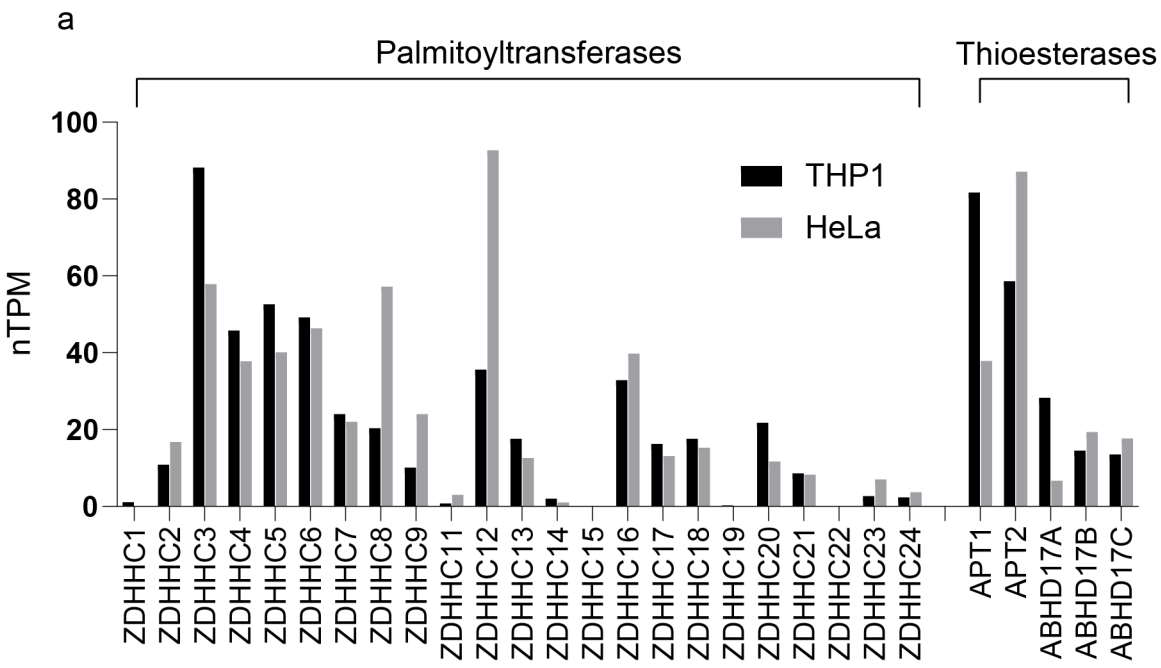

Supplementary Figure 13. Palmitoyltransferase and thioesterase transcript levels in THP-1 cells and HeLa cells. Data are collated from the human protein atlas (https://www.proteinatlas.org/).

882 **References**

883 Abrami, L., M. Audagnotto, S. Ho, M.J. Marcaida, F.S. Mesquita, M.U. Anwar, P.A. Sandoz, G. Fonti, F.
884 Pojer, M. Dal Peraro, and F.G. van der Goot. 2021. Palmitoylated acyl protein thioesterase
885 APT2 deforms membranes to extract substrate acyl chains. *Nat Chem Biol*. 17:438-447.
886 Akbal, A., A. Dernst, M. Lovotti, M.S.J. Mangan, R.M. McManus, and E. Latz. 2022. How location and
887 cellular signaling combine to activate the NLRP3 inflammasome. *Cell Mol Immunol*. 19:1201-
888 1214.
889 Andreeva, L., L. David, S. Rawson, C. Shen, T. Pasricha, P. Pelegrin, and H. Wu. 2021. NLRP3 cages
890 revealed by full-length mouse NLRP3 structure control pathway activation. *Cell*. 184:6299-
891 6312 e6222.
892 Anwar, M.U., and F.G. van der Goot. 2023. Refining S-acylation: Structure, regulation, dynamics, and
893 therapeutic implications. *J Cell Biol*. 222.
894 Apolloni, A., I.A. Prior, M. Lindsay, R.G. Parton, and J.F. Hancock. 2000. H-ras but not K-ras traffics to
895 the plasma membrane through the exocytic pathway. *Mol Cell Biol*. 20:2475-2487.
896 Breusegem, S.Y., and M.N.J. Seaman. 2014. Genome-wide RNAi screen reveals a role for multipass
897 membrane proteins in endosome-to-golgi retrieval. *Cell Rep*. 9:1931-1945.
898 Chen, J., and Z.J. Chen. 2018. PtdIns4P on dispersed trans-Golgi network mediates NLRP3
899 inflammasome activation. *Nature*. 564:71-76.
900 Chou, W.C., S. Jha, M.W. Linhoff, and J.P. Ting. 2023. The NLR gene family: from discovery to present
901 day. *Nat Rev Immunol*. 23:635-654.
902 Choy, E., V.K. Chiu, J. Silletti, M. Feoktistov, T. Morimoto, D. Michaelson, I.E. Ivanov, and M.R. Philips.
903 1999. Endomembrane trafficking of ras: the CAAX motif targets proteins to the ER and Golgi.
904 *Cell*. 98:69-80.
905 Chumpen Ramirez, S., M.R. Astrada, and J.L. Daniotti. 2020. PtdIns4P-mediated electrostatic forces
906 influence S-acylation of peripheral proteins at the Golgi complex. *Biosci Rep*. 40.
907 Davda, D., M.A. El Azzouny, C.T. Tom, J.L. Hernandez, J.D. Majmudar, R.T. Kennedy, and B.R. Martin.
908 2013. Profiling targets of the irreversible palmitoylation inhibitor 2-bromopalmitate. *ACS*
909 *Chem Biol*. 8:1912-1917.
910 Dekker, F.J., O. Rocks, N. Vartak, S. Menninger, C. Hedberg, R. Balamurugan, S. Wetzel, S. Renner, M.
911 Gerauer, B. Scholermann, M. Rusch, J.W. Kramer, D. Rauh, G.W. Coates, L. Brunsveld, P.I.
912 Bastiaens, and H. Waldmann. 2010. Small-molecule inhibition of APT1 affects Ras localization
913 and signaling. *Nat Chem Biol*. 6:449-456.
914 Duewell, P., H. Kono, K.J. Rayner, C.M. Sirois, G. Vladimer, F.G. Bauernfeind, G.S. Abela, L. Franchi, G.
915 Nunez, M. Schnurr, T. Espevik, E. Lien, K.A. Fitzgerald, K.L. Rock, K.J. Moore, S.D. Wright, V.
916 Hornung, and E. Latz. 2010. NLRP3 inflammasomes are required for atherogenesis and
917 activated by cholesterol crystals. *Nature*. 464:1357-1361.
918 Eisenberg, S., E. Haimov, G.F.W. Walpole, J. Plumb, M.M. Kozlov, and S. Grinstein. 2021. Mapping the
919 electrostatic profiles of cellular membranes. *Mol Biol Cell*. 32:301-310.
920 Ernst, A.M., S.A. Syed, O. Zaki, F. Bottanelli, H. Zheng, M. Hacke, Z. Xi, F. Rivera-Molina, M. Graham,
921 A.A. Rebane, P. Bjorkholm, D. Baddeley, D. Toomre, F. Pincet, and J.E. Rothman. 2018. S-
922 Palmitoylation Sorts Membrane Cargo for Anterograde Transport in the Golgi. *Dev Cell*.
923 47:479-493 e477.
924 Fu, J., and H. Wu. 2023. Structural Mechanisms of NLRP3 Inflammasome Assembly and Activation.
925 *Annu Rev Immunol*. 41:301-316.
926 Fukata, M., Y. Fukata, H. Adesnik, R.A. Nicoll, and D.S. Bredt. 2004. Identification of PSD-95
927 palmitoylating enzymes. *Neuron*. 44:987-996.
928 Goodwin, J.S., K.R. Drake, C. Rogers, L. Wright, J. Lippincott-Schwartz, M.R. Philips, and A.K. Kenworthy.
929 2005. Depalmitoylated Ras traffics to and from the Golgi complex via a nonvesicular pathway.
930 *J Cell Biol*. 170:261-272.

931 Gordon, D.E., L.M. Bond, D.A. Sahlender, and A.A. Peden. 2010. A targeted siRNA screen to identify
932 SNAREs required for constitutive secretion in mammalian cells. *Traffic*. 11:1191-1204.
933 Gordon, D.E., A.S. Shun-Shion, A.W. Asnawi, and A.A. Peden. 2021. Quantitative Flow Cytometry-
934 Based Assays for Measuring Constitutive Secretion. *Methods Mol Biol*. 2233:115-129.
935 Greaves, J., K.R. Munro, S.C. Davidson, M. Riviere, J. Wojno, T.K. Smith, N.C. Tomkinson, and L.H.
936 Chamberlain. 2017. Molecular basis of fatty acid selectivity in the zDHHC family of S-
937 acyltransferases revealed by click chemistry. *Proc Natl Acad Sci U S A*. 114:E1365-E1374.
938 Greaves, J., C. Salaun, Y. Fukata, M. Fukata, and L.H. Chamberlain. 2008. Palmitoylation and membrane
939 interactions of the neuroprotective chaperone cysteine-string protein. *J Biol Chem*.
940 283:25014-25026.
941 Hancock, J.F., K. Cadwallader, H. Paterson, and C.J. Marshall. 1991. A CAAX or a CAAL motif and a
942 second signal are sufficient for plasma membrane targeting of ras proteins. *EMBO J*. 10:4033-
943 4039.
944 Hancock, J.F., A.I. Magee, J.E. Childs, and C.J. Marshall. 1989. All ras proteins are polyisoprenylated
945 but only some are palmitoylated. *Cell*. 57:1167-1177.
946 Hancock, J.F., H. Paterson, and C.J. Marshall. 1990. A polybasic domain or palmitoylation is required
947 in addition to the CAAX motif to localize p21ras to the plasma membrane. *Cell*. 63:133-139.
948 Heneka, M.T., M.P. Kummer, A. Stutz, A. Delekate, S. Schwartz, A. Vieira-Saecker, A. Griep, D. Axt, A.
949 Remus, T.C. Tzeng, E. Gelpi, A. Halle, M. Korte, E. Latz, and D.T. Golenbock. 2013. NLRP3 is
950 activated in Alzheimer's disease and contributes to pathology in APP/PS1 mice. *Nature*.
951 493:674-678.
952 Heo, W.D., T. Inoue, W.S. Park, M.L. Kim, B.O. Park, T.J. Wandless, and T. Meyer. 2006. PI(3,4,5)P3 and
953 PI(4,5)P2 lipids target proteins with polybasic clusters to the plasma membrane. *Science*.
954 314:1458-1461.
955 Hochheiser, I.V., M. Pilsl, G. Hagelueken, J. Moecking, M. Marleaux, R. Brinkschulte, E. Latz, C. Engel,
956 and M. Geyer. 2022. Structure of the NLRP3 decamer bound to the cytokine release inhibitor
957 CRID3. *Nature*. 604:184-189.
958 Hornung, V., F. Bauernfeind, A. Halle, E.O. Samstad, H. Kono, K.L. Rock, K.A. Fitzgerald, and E. Latz.
959 2008. Silica crystals and aluminum salts activate the NALP3 inflammasome through
960 phagosomal destabilization. *Nat Immunol*. 9:847-856.
961 Jennings, B.C., and M.E. Linder. 2012. DHHC protein S-acyltransferases use similar ping-pong kinetic
962 mechanisms but display different acyl-CoA specificities. *J Biol Chem*. 287:7236-7245.
963 Jennings, B.C., M.J. Nadolski, Y. Ling, M.B. Baker, M.L. Harrison, R.J. Deschenes, and M.E. Linder. 2009.
964 2-Bromopalmitate and 2-(2-hydroxy-5-nitro-benzylidene)-benzo[b]thiophen-3-one inhibit
965 DHHC-mediated palmitoylation in vitro. *J Lipid Res*. 50:233-242.
966 Kathayat, R.S., Y. Cao, P.D. Elvira, P.A. Sandoz, M.E. Zaballa, M.Z. Springer, L.E. Drake, K.F. Macleod,
967 F.G. van der Goot, and B.C. Dickinson. 2018. Active and dynamic mitochondrial S-
968 depalmitoylation revealed by targeted fluorescent probes. *Nat Commun*. 9:334.
969 Koulouras, G., A. Panagopoulos, M.A. Rapsomaniki, N.N. Giakoumakis, S. Taraviras, and Z. Lygerou.
970 2018. EasyFRAP-web: a web-based tool for the analysis of fluorescence recovery after
971 photobleaching data. *Nucleic Acids Res*. 46:W467-W472.
972 Laude, A.J., and I.A. Prior. 2008. Palmitoylation and localisation of RAS isoforms are modulated by the
973 hypervariable linker domain. *J Cell Sci*. 121:421-427.
974 Lee, B., C. Hoyle, R. Wellens, J.P. Green, F. Martin-Sanchez, D.M. Williams, B.J. Matchett, P.I. Seoane,
975 H. Bennett, A. Adamson, G. Lopez-Castejon, M. Lowe, and D. Brough. 2023. Disruptions in
976 endocytic traffic contribute to the activation of the NLRP3 inflammasome. *Sci Signal*.
977 16:eabm7134.
978 Lemonidis, K., M.W. Werno, J. Greaves, C. Diez-Ardanuy, M.C. Sanchez-Perez, C. Salaun, D.M.
979 Thomson, and L.H. Chamberlain. 2015. The zDHHC family of S-acyltransferases. *Biochem Soc*
980 *Trans*. 43:217-221.

981 Liang, J.J., I.D.C. Fraser, and C.E. Bryant. 2021. Lipid regulation of NLRP3 inflammasome activity
982 through organelle stress. *Trends Immunol*. 42:807-823.
983 Lin, D.T., and E. Conibear. 2015. ABHD17 proteins are novel protein depalmitoylases that regulate N-
984 Ras palmitate turnover and subcellular localization. *Elife*. 4:e11306.
985 Linder, M.E., P. Middleton, J.R. Hepler, R. Taussig, A.G. Gilman, and S.M. Mumby. 1993. Lipid
986 modifications of G proteins: alpha subunits are palmitoylated. *Proc Natl Acad Sci U S A*.
987 90:3675-3679.
988 Lv, D., X. Cao, L. Zhong, Y. Dong, Z. Xu, Y. Rong, H. Xu, Z. Wang, H. Yang, R. Yin, M. Chen, C. Ke, Z. Hu,
989 W. Deng, and B. Tang. 2023. Targeting phenylpyruvate restrains excessive NLRP3
990 inflammasome activation and pathological inflammation in diabetic wound healing. *Cell Rep*
991 *Med*. 4:101129.
992 Mateo-Tórtola, M., I.V. Hochheiser, J. Grga, J.S. Mueller, M. Geyer, A.N.R. Weber, and A. Tapia-Abellán.
993 2023. Non-decameric NLRP3 forms an MTOC-independent inflammasome.
994 *bioRxiv*:2023.2007.2007.548075.
995 Michaelson, D., J. Silletti, G. Murphy, P. D'Eustachio, M. Rush, and M.R. Philips. 2001. Differential
996 localization of Rho GTPases in live cells: regulation by hypervariable regions and RhoGDI
997 binding. *J Cell Biol*. 152:111-126.
998 Munoz-Planillo, R., P. Kuffa, G. Martinez-Colon, B.L. Smith, T.M. Rajendiran, and G. Nunez. 2013. K(+)
999 efflux is the common trigger of NLRP3 inflammasome activation by bacterial toxins and
1000 particulate matter. *Immunity*. 38:1142-1153.
1001 Ohno, Y., A. Kihara, T. Sano, and Y. Igarashi. 2006. Intracellular localization and tissue-specific
1002 distribution of human and yeast DHHC cysteine-rich domain-containing proteins. *Biochim*
1003 *Biophys Acta*. 1761:474-483.
1004 Perregaux, D., J. Barberia, A.J. Lanzetti, K.F. Geoghegan, T.J. Carty, and C.A. Gabel. 1992. IL-1 beta
1005 maturation: evidence that mature cytokine formation can be induced specifically by nigericin.
1006 *J Immunol*. 149:1294-1303.
1007 Rivera, V.M., X. Wang, S. Wardwell, N.L. Courage, A. Volchuk, T. Keenan, D.A. Holt, M. Gilman, L. Orci,
1008 F. Cerasoli, Jr., J.E. Rothman, and T. Clackson. 2000. Regulation of protein secretion through
1009 controlled aggregation in the endoplasmic reticulum. *Science*. 287:826-830.
1010 Rocks, O., M. Gerauer, N. Vartak, S. Koch, Z.P. Huang, M. Pechlivanis, J. Kuhlmann, L. Brunsveld, A.
1011 Chandra, B. Ellinger, H. Waldmann, and P.I. Bastiaens. 2010. The palmitoylation machinery is
1012 a spatially organizing system for peripheral membrane proteins. *Cell*. 141:458-471.
1013 Rocks, O., A. Peyker, M. Kahms, P.J. Verveer, C. Koerner, M. Lumbierres, J. Kuhlmann, H. Waldmann,
1014 A. Wittinghofer, and P.I. Bastiaens. 2005. An acylation cycle regulates localization and activity
1015 of palmitoylated Ras isoforms. *Science*. 307:1746-1752.
1016 Rollins, C.T., V.M. Rivera, D.N. Woolfson, T. Keenan, M. Hatada, S.E. Adams, L.J. Andrade, D. Yaeger,
1017 M.R. van Schravendijk, D.A. Holt, M. Gilman, and T. Clackson. 2000. A ligand-reversible
1018 dimerization system for controlling protein-protein interactions. *Proc Natl Acad Sci U S A*.
1019 97:7096-7101.
1020 Roy, M.O., R. Leventis, and J.R. Silvius. 2000. Mutational and biochemical analysis of plasma
1021 membrane targeting mediated by the farnesylated, polybasic carboxy terminus of K-ras4B.
1022 *Biochemistry*. 39:8298-8307.
1023 Salaun, C., J. Greaves, and L.H. Chamberlain. 2010. The intracellular dynamic of protein palmitoylation.
1024 *J Cell Biol*. 191:1229-1238.
1025 Schindelin, J., I. Arganda-Carreras, E. Frise, V. Kaynig, M. Longair, T. Pietzsch, S. Preibisch, C. Rueden,
1026 S. Saalfeld, B. Schmid, J.Y. Tinevez, D.J. White, V. Hartenstein, K. Eliceiri, P. Tomancak, and A.
1027 Cardona. 2012. Fiji: an open-source platform for biological-image analysis. *Nat Methods*.
1028 9:676-682.
1029 Schmacke, N.A., F. O'Duill, M.M. Gaidt, I. Szymanska, J.M. Kamper, J.L. Schmid-Burgk, S.C. Madler, T.
1030 Mackens-Kiani, T. Kozaki, D. Chauhan, D. Nagl, C.A. Stafford, H. Harz, A.L. Frohlich, F. Pinci, F.
1031 Ginhoux, R. Beckmann, M. Mann, H. Leonhardt, and V. Hornung. 2022. IKKbeta primes

1032 inflammasome formation by recruiting NLRP3 to the trans-Golgi network. *Immunity*. 55:2271-
1033 2284 e2277.
1034 Schmick, M., N. Vartak, B. Papke, M. Kovacevic, D.C. Truxius, L. Rossmannek, and P.I.H. Bastiaens. 2014.
1035 KRas localizes to the plasma membrane by spatial cycles of solubilization, trapping and
1036 vesicular transport. *Cell*. 157:459-471.
1037 Seoane, P.I., B. Lee, C. Hoyle, S. Yu, G. Lopez-Castejon, M. Lowe, and D. Brough. 2020. The NLRP3-
1038 inflammasome as a sensor of organelle dysfunction. *J Cell Biol*. 219.
1039 Swanson, K.V., M. Deng, and J.P. Ting. 2019. The NLRP3 inflammasome: molecular activation and
1040 regulation to therapeutics. *Nat Rev Immunol*. 19:477-489.
1041 Swarthout, J.T., S. Lobo, L. Farh, M.R. Croke, W.K. Greentree, R.J. Deschenes, and M.E. Linder. 2005.
1042 DHHC9 and GCP16 constitute a human protein fatty acyltransferase with specificity for H- and
1043 N-Ras. *J Biol Chem*. 280:31141-31148.
1044 Tapia-Abellan, A., D. Angosto-Bazarra, C. Alarcon-Vila, M.C. Banos, I. Hafner-Bratkovic, B. Oliva, and P.
1045 Pelegrin. 2021. Sensing low intracellular potassium by NLRP3 results in a stable open structure
1046 that promotes inflammasome activation. *Sci Adv*. 7:eabf4468.
1047 Tomatis, V.M., A. Trenchi, G.A. Gomez, and J.L. Daniotti. 2010. Acyl-protein thioesterase 2 catalyzes
1048 the deacylation of peripheral membrane-associated GAP-43. *PLoS One*. 5:e15045.
1049 Toyoda, T., H. Sugimoto, and S. Yamashita. 1999. Sequence, expression in Escherichia coli, and
1050 characterization of lysophospholipase II. *Biochim Biophys Acta*. 1437:182-193.
1051 Vartak, N., B. Papke, H.E. Grecco, L. Rossmannek, H. Waldmann, C. Hedberg, and P.I. Bastiaens. 2014.
1052 The autodepalmitoylating activity of APT maintains the spatial organization of palmitoylated
1053 membrane proteins. *Biophys J*. 106:93-105.
1054 Wang, A., R.A. Deems, and E.A. Dennis. 1997. Cloning, expression, and catalytic mechanism of murine
1055 lysophospholipase I. *J Biol Chem*. 272:12723-12729.
1056 Wang, L., J. Cai, X. Zhao, L. Ma, P. Zeng, L. Zhou, Y. Liu, S. Yang, Z. Cai, S. Zhang, L. Zhou, J. Yang, T. Liu,
1057 S. Jin, and J. Cui. 2023. Palmitoylation prevents sustained inflammation by limiting NLRP3
1058 inflammasome activation through chaperone-mediated autophagy. *Mol Cell*. 83:281-297
1059 e210.
1060 Webb, Y., L. Hermida-Matsumoto, and M.D. Resh. 2000. Inhibition of protein palmitoylation, raft
1061 localization, and T cell signaling by 2-bromopalmitate and polyunsaturated fatty acids. *J Biol*
1062 *Chem*. 275:261-270.
1063 Won, S.J., M. Cheung See Kit, and B.R. Martin. 2018. Protein depalmitoylases. *Crit Rev Biochem Mol*
1064 *Biol*. 53:83-98.
1065 Yeung, T., G.E. Gilbert, J. Shi, J. Silvius, A. Kapus, and S. Grinstein. 2008. Membrane phosphatidylserine
1066 regulates surface charge and protein localization. *Science*. 319:210-213.
1067 Yu, T., D. Hou, J. Zhao, X. Lu, W.K. Greentree, Q. Zhao, M. Yang, D.-G. Conde, M.E. Linder, and H. Lin.
1068 2023. NLRP3 Cys126 palmitoylation by ZDHHC7 Promotes Inflammasome Activation.
1069 *bioRxiv*:2023.2011.2007.566005.
1070 Zhang, Z., R. Venditti, L. Ran, Z. Liu, K. Vivot, A. Schurmann, J.S. Bonifacino, M.A. De Matteis, and R.
1071 Ricci. 2023. Distinct changes in endosomal composition promote NLRP3 inflammasome
1072 activation. *Nat Immunol*. 24:30-41.
1073 Zhou, Y., P. Prakash, A.A. Gorfe, and J.F. Hancock. 2018. Ras and the Plasma Membrane: A Complicated
1074 Relationship. *Cold Spring Harb Perspect Med*. 8.
1075 Zhou, Y., P. Prakash, H. Liang, K.J. Cho, A.A. Gorfe, and J.F. Hancock. 2017. Lipid-Sorting Specificity
1076 Encoded in K-Ras Membrane Anchor Regulates Signal Output. *Cell*. 168:239-251 e216.

1077